# Morphodynamic modelling with suspended sediment transport in river bends

Master of Science Thesis
Department of Civil Engineering
Delft University of Technology

Ioannis Arailopoulos
November 2014

TU Delft

Deltares
Enabling Delta Life

# Morphodynamic modelling with suspended sediment transport in river bends

Master of Science Thesis
Department of Civil Engineering
Delft University of Technology

Ioannis Arailopoulos
November 2014

TU Delft

Deltares
Enabling Delta Life

Graduation committe:

| | |
|---|---|
| Prof.dr.ir. Zheng Bing Wang | Delft University of Technology, Deltares |
| Dr.ir. Erik Mosselman | Delft University of Technology, Deltares |
| Dr.ir. Kees Sloff | Delft University of Technology, Deltares |

Keywords: river morphodynamics, suspended sediment, secondary flow, Delft3D.

Κριτήριον τόν λόγον,
τάς αἰσθήσεις μή ακριβεῖς ὑπάρχειν.
Παρμενίδης

Στους γονείς μου.

# Preface

Physical sciences try to explain the existence of time through physical laws. The prevailing theory regarding the direction of time and life evolution is related to the second law of thermodynamics and the concept of maximum entropy. Entropy is a state function which shows in how many ways a system can be rearranged, also regarded as a meter for the degree of 'disorder'. The most probable state of a system is the one with the highest 'disorder', or the highest amount of entropy. A formal evidence of the theory can be found inside the concept of the hydrological cycle. In the first part of the cycle we face disorder of water mass towards the most probable state of water distribution by the rainfalls which follow the processes of evaporation and interception. The second part of the cycle results in friction forces and the transport of grains resulting in disorder of soil mass. Major role on this system have the rivers. Not unfairly, they have been called "the arteries of our planet". The main reason is not this role but other, more pragmatic ones exist which also trigger the need for their investigation. They support life of flora and fauna from the early times. Nowadays humans use them not only as a source of fresh water, but also of electric power, or as waterways, and take advantage of their fertility in the riparian zone. This fertility is an immediate result of flooding events and changes in the river planforms. But flooding is one of the main natural disasters that mankind has to be protected from. This makes people often forget or not care about its positive results. From both fertility and flooding emerged the need for measures necessary for ensuring safety and navigability.

Today's era is unofficially called the anthropocene. It is commonly accepted that human activity influences the earth's ecosystem. On the one hand, this influence facilitates rapid changes, and quicker morphological processes, which people try to sustain, and on the other hand a total prevention of floods and planform evolution can have catastrophic effects on the natural ecosystem. Nowadays active measure policies have become ambiguous, and a passive policy often seems more reasonable to be adopted. The above impel the investigation of river patterns more than ever. A necessary component for proper prediction of their behaviour is the morphological bed evolution, a topic directly connected with this study.

A reader may not be particularly interested in the 'philophronetic expressions' by the author, but personally I find this section one of the last that could be missing from this thesis. I would like to thank Kees Sloff for his support and guidance, and not just a few times I knew that he was the only one that could answer my questions in a way clear for me. I also have to praise his sense of humour that made my stay at Deltares even more enjoyable. I am grateful to my professor Zheng B. Wang, and impressed by his inspiring way of thinking. A special thank you is for Erik Mosselman, the person who became my

mentor, not only through his extensive help and support for producing the present thesis, but also for his guidance on more personal issues. I also want to thank Willem Ottevanger for his assistance from the first moment I arrived at Deltares, giving me access to his work, and helping me without return, even when he was extremely busy just a few weeks before his PhD defence. Finally, I want to thank all the people, inside and outside Deltares, who made the Netherlands feel like 'home'.

*Delft, November 2014* Ioannis Arailopoulos

# Summary

Keywords: river morphodynamics, suspended sediment, secondary flow, Delft3D.

Depth-averaged morphological computations using Delft3D tend to produce 'strange', results for river bends when the sediment transport formulas of Van Rijn are used. Even pools in inner bend regions and bars in outer bend regions can result from the model. The objective of the present thesis is to identify the cause of the problem and propose potential solutions.

A short analysis shows that the 'strange' predictions are not connected to the Van Rijn's formulations, but to suspended sediment transport modelling in general. An axi-symmetric solution (viz. the equilibrium solution of the transverse slope in an infinitely long bend with constant width and curvature) is derived for the case where suspended sediment transport is included, based on a formulation for the bed load transport by Olesen (1987). It is indicated that the limitations of the model including suspended sediment transport, along with bad modelling practices, can produce unrealistic results. Delft3D implicitly models the influence of secondary flow on the suspended sediment transport with the help of a mixing coefficient. Numerical experiments show that this is not possible in a river bend context, unless calibrating the parameters in such a way that they would lose their physical meaning. In order to overcome this problem, it is concluded that the influence of secondary flow on the suspended sediment has to be modelled explicitly.

A suspended sediment transport model is designed, which includes the influence of secondary flow due to the variation in vertical direction of the profiles of secondary flow and suspended sediment. The depth-averaged expressions including the dispersion of suspended sediment by the main and the secondary flow are derived by using analytical similarity profiles of sediment concentration ($0^{th}$ order Rouse profile) and secondary flow (Kalkwijk & Booij, 1986) for closing the extra terms. These expressions are implemented in Delft3D and the resulting code is used to carry out numerical simulations for hypothetical and real test cases including flume experiments.

The analysis is confirmed by the simulations and the results of the improved depth-averaged code are much more realistic (from a mathematical point of view) as they show, especially for the hypothetical test cases, good agreement with the results from 3D computations (using also Delft3D). On the other hand, the applicability of the model to cases with large curvatures is more problematic, unless a more accurate expression for the secondary flow is used.

It is concluded that incorporating the influence of secondary flow on the direction of suspended sediment along with the option of using a distribution function with variable

shape is highly beneficial for morphological modelling in river bends. Another alternative is indicated to be the appropriate calibration of the morphological model. This is a less viable option, as it could even lead on disconnecting parameters from their physical meaning.

# Contents

# Chapter 1

# Introduction

Engineering is traditionally a field strongly related to empirical observations, experimental results, and mathematical treatment of physical laws for deriving analytical expressions. Until recently, these where the main available tools, and this gave their treatment a high potential. In this way they became strong foundations for the involvement of computer science. Still, it is not possible to find analytical solutions to the complete Navier-Stokes equations which form the basis of fluid dynamics. During the last century, numerical analysis through computational fluid dynamics (CFD) became a feasible tool for discrete solving of equations that describe complex processes, and now it stands equal, next to experiments and theoretical analysis (Wendt, 2009). Nowadays, the role of scaled models is twofold. It is still at the edge of understanding physical concepts, and at the same time it is used for calibrating numerical models. On the other hand, the reliance on them in engineering practice is reducing (while computer power increases), mainly due to financial and time costs.

The accuracy and applicability of this 'new' tool is questioned by a part of the scientific community. Bigger concerns emerge inside the world of morphodynamic computations using CFD, where also this research lies in. Fundamental physical laws for describing the water flow and the interaction with the soil have been realized almost 2 centuries ago. These can be solved in a discrete manner using CFD, but the biggest constraint until today is time. Morphological computations that are slower than the actual processes are rarely relevant for a morphologist. Simplifying assumptions, necessary for minimizing the computational time, sacrifice some of the accuracy of the end result. A large part of the research community tries to identify which assumptions are the most relevant. The cost that commonly follows them is the sensitivity of model results to empirical and calibrating parameters. Truncation and round-off errors have to be added, that impact the accuracy. In addition, nothing would make sense without a proper and accurate description of the physical conditions, sometimes for the past, and usually for the present and the future. Skepticism regarding

large-scale morphodynamics using CFD is as a result well justified. Still, practise shows that a balance point exists between absolute and zero accuracy (or the more relevant 'rule of thumb' accuracy), where the information to the policy makers is beneficial and even decisive. Modern management techniques demand them and their development is highly relevant. Moreover, concepts can be derived, and processes can be identified, at scales that would be impossible with physical experiments by current means. The present study has a goal to identify such a balance.

The cause that initiated the present research was the inapplicability of a specific morphodynamic modelling suite, Delft3D, in specific environments, when applying the sediment transport formulas of Van Rijn. The final objectives could not have been formulated beforehand. The analysis pointed out that the context is more general. Morphological modelling including suspended sediment transport in rivers, using Delft3D, can potentially produce inaccurate and even unrealistic predictions, unless special attention is given, even in cases where the model is in principle valid. As a result, it was decided that also the importance of the processes driving the suspended sediment transport had to be investigated.

Although it may seem that the study subject is confined to a particular morphological model, it is also relevant for models developed on similar principles as Delft3D. Moreover, it seeks to provide useful information for river modellers, discussing when it can be relevant to include suspended sediment transport in their models (regarding geometries and not phenomena, i.e. tidal influence), and which would be the most appropriate way to do so under current means. In particular, it tries to explore the possibilities of modelling suspended sediment in a depth-averaged context, in curved alluvial channels.

## 1.1 Background and context

A morphological study was performed for the Rio Atrato, a river situated in Colombia, by Melman (2011), for investigating the possibilities of creating an inter-oceanic waterway connection between the Pacific ocean and the Caribbean sea. With focus on an unstable bifurcation of the river (Montaño-Murindó bifurcation), a 2D depth-averaged morphological model was developed, in Delft3D. The reach in the vicinity of that region is characterized by mild to sharp bends, and relatively fine sediment ($D_{50} \approx 0.10 - 0.35\,\text{mm}$ depending on the measurement data). In a sensitivity analysis that he performed, it was evident that, when applying in the model the sediment transport formulas of Van Rijn, the results were unrealistic. For the equilibrium solution (solution with no changes in time), even pools in the inner bend regions and bars in the outer bend regions were modelled. Melman (2011) credited this 'strange' behaviour to the formula applied, as the predictions using other formulas (Engelund & Hansen, 1967; Meyer-Peter & Müller, 1948) were realistic and similar


Figure 1.1: Bed levels after 100 years of morphological changes using different sediment transport predictors in Rio Atrato, Colombia (Melman, 2011).

between them. Also the implementation of the formula to the software was questioned but the chances of such an error were minimized after thorough investigation of the algorithm by Deltares.

It is common to divide the sediment load into two modes of transport, bed load and suspended load. This is a conceptual distinction, and different definitions exist on how to distinguish them. The reader who is unfamiliar with morphological models including suspended sediment transport in an alluvial river context is referenced to Chapter 2 of the present thesis, and for even more details on the subject to Mosselman (2005) and Wu (2007). Practically, a reference height starting from the bed is chosen inside the water column which divides the two modes, with suspended load being the one above it. Bed load is usually assumed to instantaneously adapt to the local flow conditions, whereas suspended load responds in a time and space lag manner, related to the time needed for a grain in suspension to reach the bed. Sediment transport models either do not distinguish the two modes, or ignore the suspended sediment transport. When there is no clear distinction, suspended load and bed load are usually considered as one (both are modelled as bed load). As a result, total load formulas can be applied in models as bed load formulas, with the Engelund and Hansen (1967) formula a common example. The sediment transport model of Van Rijn is the only one (from the three that were applied in the Rio Atrato) that explicitly distinguishes the suspended sediment load from the bed load. Still, at this point there is no

connection between the 'strange' behaviour of Delft3D using the formulas of Van Rijn and suspended sediment transport modelling.

It is generally assumed that suspended sediment follows the water flow velocity except in the vertical where it 'slips' with a fall velocity driven by the different specific densities of water and soil. This concept may be misleading, especially in a depth-averaged sense, as the suspended sediment does not follow the depth-averaged velocity, but is further influenced by a dispersive (transport due to the deviation from a uniform distribution of the velocity in the horizontal plane and the suspended sediment concentration) and a diffusive transport component (transport due to turbulent velocity and concentration fluctuations in time). These two mechanisms can be important for morphological predictions (Z. B. Wang, 1989). Although their magnitudes may be much smaller than the component of suspended sediment transport in the direction of the depth-averaged velocity, they can be crucial as they form a transport component normal to it, which can strongly influence morphological patterns along the cross-stream direction. According to Wu (2007) 'in curved channels, the dispersion fluxes become important and need to be modelled.' In depth-averaged modelling using Delft3D, dispersion and diffusion are not modelled separately, and the diffusive stresses represent both effects (with the help of a mixing coefficient).

## 1.2 Problem statement and research objectives

It was realized, as already stated, that depth-averaged modelling using Delft3D and the sediment transport formulas of Van Rijn can produce 'strange' morphological results. Even pools in inner-bend regions and bars in outer-bend regions can be modelled. The reasons behind this are not understood. Moreover, research shows that it is important to model dispersion and diffusion of suspended sediment separately in a depth-averaged river bend context. The processes are not implemented in Delft3D in such a way and this can be a cause of unrealistic morphological predictions. Finally, whether these two problems are connected is not known.

Two objectives are formed immediately emerging from the predefined problems. The first is understanding the reasons behind the 'strange' morphological predictions in river bends when using Delft3D and the Van Rijn's sediment transport formulas. The second is to investigate the possibilities of modelling the influence of secondary flow on the suspended sediment transport in Delft3D in an explicit way.

The questions being posed are:

- Is the 'strange' behaviour a result of Van Rijn's formulations or is there another reason?

- Will a separate treatment of dispersion and diffusion in the depth-averaged version of Delft3D produce more accurate results in a river bend context?

Research regarding the application of Van Rijn's formulas is highly relevant. The fact that they are commonly used in real case studies proves their importance. Moreover, this investigation can provide further insight into problems and best practices in morphological modelling in river bends. The goal is to help enhancing the confidence of modellers in such environments.

Modelling suspended sediment is computationally much more demanding than modelling only bed load transport. An extra second-order differential equation is added to the system of equations describing the water flow processes and bed level changes. It is relevant to ignore, if possible, suspended sediment load (model it in the same as bed load) in a river context. The relatively small adaptation lengths of suspended sediment in comparison with the dimensions of grid cells commonly applied in numerical models can generally justify this assumption in straight reaches (Mosselman, 2005). If this is the case for river bends, this research could still be interesting for understanding the relevant importance of physical processes, but would not have high practical importance. Firstly, physical experiments show that an increase in the transverse slopes is expected in cases with suspended sediment transport in river bends (Talmon, 1992). Moreover, the linear analyses of Olesen (1987) and Talmon (1992) show that suspended sediment transport can have a striking influence on the wave length and damping of the solution of the bed topography. More details of the analysis by Talmon (1992) are included in Chapter 2. These are only a few reasons among other ones that can justify the importance of suspended sediment transport modelling.

## 1.3 Methodology and outline

Two different methodologies are needed to answer, at least at this point, two different questions. The first objective regarding the Van Rijn formula is investigated by means of several test cases. The results of every step determine the whole methodology which is not known a priori. The source of errors is researched by deconstructing the components that influence the solution. An analysis of the axi-symmetric solution (viz. the equilibrium solution of an infinitely long bend with constant width and curvature) in river bends in cases with suspended sediment load becomes relevant, and is used for explaining problems related to the application of the formulas. A simple relation for the bed load is used, as described by Olesen (1987), in order to perform the analysis. In order to reach the second objective and acknowledge the influence of dispersion, a suspended sediment model is designed. The depth-averaged expressions for the effects of secondary flow are based on similarity profiles of sediment concentration ($0^{th}$ order Rouse profile), main (Kalkwijk

& De Vriend, 1980), and secondary flow (Kalkwijk & Booij, 1986). The higher-order contributions to the suspended sediment concentration are assumed not to be important for the influence of secondary flow and are neglected without further proof. Both the influence on the concentration field (convection-diffusion equation of suspended sediment) and the sediment transport direction are implemented in Delft3D. The resulting code is used to carry out numerical simulations for hypothetical and real bends and the results are compared with three-dimensional equations with the same base settings, also using Delft3D, or with flume experiments, when relevant.

The general theoretical framework, with a quick reference to the principles of morphodynamic modelling using CFD under the context of the present study (for a more detailed approach the reader is referred to Appendix A), and analyses of modelling suspended sediment transport are included in the following chapter (Chapter 2). The applicability of Van Rijn's formulas in river bends using Delft3D and the source of unrealistic predictions is investigated in Chapter 3. An analysis of the influence of secondary flow on the axi-symmetric solution, which enhances understanding of the problems related with application of the Van Rijn's formulas, is included in the same chapter. The derivation of a suspended sediment transport model which is implemented in Delft3D, the shortcomings of the implementation and the approach, and the results from numerical experiments testing the modified model are presented in Chapter 4. Finally, the conclusions and recommendations are stated on the last chapter (Chapter 5).

# Chapter 2

# General framework

The present research regards modelling morphodynamic processes using CFD, with focus on curved open channels. Except for the difficulty of predicting the water flow, a new dimension is added, which increases the complexity of the system. Studying river morphodynamics involves understanding the influence of water movement on the adjacent soil and vice versa. The mechanisms are conceptualized and divided into the flow distribution, the sediment transport, and the bed level variations (Jansen, Van Bendegom, Van den Berg, De Vries, & Zanen, 1979).

Natural rivers tend to meander. These meanders are responsible for complicated processes that we started to understand after the middle of the $19^{\text{th}}$ century with the help of Boussinesq (1868). Then it was the first time that the curved open channel flow was treated mathematically. The difference in the balance between inertial with pressure forces in their vertical profiles was found to be the cause for a weak, yet important for morphological predictions, velocity, normal to the depth-averaged velocity, called the secondary (or spiral) flow. Two revolutionary studies performed by Ananyan (1965, orig. publ. in Russian 1957) and Rozovskii (1961, orig. publ. in Russian 1957) opened the way for deriving analytical solutions for curved-channel flow using perturbation methods to the mass and momentum balance equations. After the mature mathematical analysis of this period De Vriend (1981) developed a mathematical model, which was used as a basis for depth-averaged numerical solving of water flow in river bends. Increasing computer power led to more complex mathematical models which could be solved numerically. In 3-dimensional models, the water velocity field is in principle solved and there is no need for secondary-flow closure models. Recently, the simulation of the fully three-dimensional flow pattern in curved open channels has become possible with advanced numerical models (with ascending accuracy and descending magnitude of the empirical factor from Reynolds-averaged Navier-Stokes, with a turbulence closure model e.g. nonlinear k-$\epsilon$, to large-eddy simulation, and direct numerical simulation) (Ottevanger, 2013).

A morphologist has to define a distinction between the modes of sediment transport. The precise division has minor physical meaning, but aids in gaining a better insight into the physical processes. Sediment transport is divided in regard to its source and its transport mechanism (Jansen et al., 1979). According to the transport mechanism distinction, we define bed load and suspended load. Van Rijn (1984a, 1984b, 1984c) distinguishes two different ways that this definition takes place. The first, as proposed by Bagnold (1941, 1973) defines "the bed load transport as that in which the successive contacts of the particles with the bed are strictly limited by the effect of gravity, while the suspended load transport is defined as that in which the excess weight of the particles is supported wholly by a random succession of upward impulses imparted by turbulent eddies." The latter, now by Einstein (1950) defines "the bed load transport as the transport of sediment particles in a thin layer of 2 particle diameters thick just above the bed by sliding, rolling and sometimes by making jumps with a longitudinal distance of a few particle diameters."

The transport of sediment is almost always treated on a macroscopic level, especially for small grain sizes. We are not interested in the trajectory of each grain individually, but of sediment as a whole. At this level, strongly semi-empirical formulations are necessary for estimating the sediment transport capacity of the flow. The study on the mobility of sediment by Shields (1936) identified the movement of sediment on a macroscopic level. Meyer-Peter and Müller (1948) and Einstein (1950) focused on defining the amount of the transported sediment (although historically they were not the first). Based on their work, important sediment formulas, used for predicting transport capacities and widely applied in river morphology, were derived. This capacity is not always assumed to be equal to the estimated sediment transport due to relaxation effects. This is important especially for suspended sediment transport. For an in-depth analysis on sediment transport modelling reference is made to Mosselman (2005).

Bed level variations can be computed by means of a mass balance equation which can be based either on the exchange of sediment between the bed and the flow, or on the total sediment transport gradient. A quasi-steady bed can be assumed for every time step of hydrodynamic computations (De Vries, 1959, 1965; Jansen et al., 1979). This is generally valid for $Fr < 0.8$. With this assumption it is possible to decouple the hydrodynamic equations from the bed level variations, something that enhances the computational speed of the system.

Modelling accuracy is strongly correlated with simulation time. High-precision models are not yet common in large-scale engineering practice. For long-term morphological predictions, in large model domains, less complex but computationally more efficient solutions have to be applied. In the case of curved open channel flow, the 3D spiral flow structure is not captured after depth averaging. The influence of the velocity field is lost

if we assume that the square of the depth-averaged velocity is equal to the square of the actual velocity integrated over the depth. This results in neglecting dispersion stresses. For non-curved flow with constant channel width, this assumption is not that crude, because we can assume that these stresses are incorporated inside the turbulence closure model due to their relatively small spatial and time variations (by adding the influence to the turbulent viscosity coefficient). This is not possible in the case of curved flow, as this influence is different throughout the bend causing a complex re-distribution of momentum. A computationally efficient secondary-flow model valid within the mild-curvature limit was derived by Kalkwijk and Booij (1986), whereas Blanckaert (2002) derived a model applicable in sharper bends.

Of crucial importance is the influence the secondary flow has on river morphology due to two effects. It causes the deviation between the depth-averaged flow velocity and the bed shear stress, which is considered the driving force of the bed load due to water flow (along with the bed slope effects). This is easily understood if a velocity would be calculated by averaging over a layer near the bed and not in the whole water column. The second is that because of the non-uniform distribution of the suspended sediment that we normally encounter, the flow pattern causes the deviation of its direction from the depth-averaged velocity (along with diffusion). This process is similar to the dispersion of flow momentum, but now there is dispersion of suspended sediment. For an extended analysis on the first subject, reference is made to Olesen (1987), while for the latter reference is made to Z. B. Wang (1989), Talmon (1992), Wu and S. S. Y. Wang (2005), and Huang, Jia, and Wang (2006).

Except for the dispersion stresses that have to be closed (and become important in curved flow) another major difficulty that arises in a 2DH suspended sediment transport model is the calculation of the exchange of sediment with the bed load zone. This boundary condition determines the quantity of sediment in the water column. It can be applied in two ways, by assuming that either the concentration or the flux of the concentration in the vertical at the bottom instantaneously adapts to the equilibrium condition. Both conditions usually demand the need for semi-empirical relations, as neither the vertical concentration profile nor the near-bed sediment concentration is computed. This is not the case after Galappatti (1983), who applied an asymptotic approximation to the 2DV mass balance. The theory of Galappatti was generalized by Z. B. Wang (1989). Talmon (1992), also following Galappatti's theory, proposed a depth-averaged 2D model after expressing the 3D mass balance in a cylindrical coordinate system. In this way, the vertical sediment concentration profile can be computed with minor dependence on the empirical factor (secondary flow and vertical diffusion coefficient profile still necessary). The dispersion stresses in curved open channels do not only need a semi-empirical profile for the suspended

sediment concentration, but they also need profiles for the secondary flow and the vertical diffusion coefficient.

A more detailed description of the processes is included in Appendix A for the reader who is unfamiliar with morphological modelling.

## 2.1 Linear analysis of morphological modelling including suspended sediment transport

A critical question is whether suspended sediment transport actually influences morphological predictions in river bends. A linear analysis of the system of equations for water, sediment transport, and bed level changes can answer the influence on the wavenumber and damping of the solution. A semi-forced and a freely migrating alternate bar analysis was performed by Talmon (1992) and its results are remarkable. For full description of the analyses reference is made to Talmon (1992). An introduction to the first follows. In short:

- the curvature of the coordinate system is neglected (no extra terms), the influence of secondary flow and of diffusion is neglected, and only the momentum equation in $s$ direction is taken into account in the analysis (neglect momentum equation in transverse direction),

- the remaining equations of the system represent the continuity equations for water and sediment (Exner principle), the convection equation of suspended sediment, and the depth-averaged equilibrium concentration.

Three important adaptation lengths are defined, of the main flow ($\lambda_w$), the bed level ($\lambda_s$), and the depth-averaged concentration ($\lambda_c$). They read, respectively,

$$\lambda_w = \frac{C^2}{2g} h_0 \tag{2.1}$$

$$\lambda_s = \frac{1}{\pi^2} \left( \frac{W}{h_0} \right)^2 f(\theta) h_0 \tag{2.2}$$

$$\lambda_c = L_a \frac{u_0}{w_s} h_0 \tag{2.3}$$

where

| | |
|---|---|
| $C$ | Chézy smoothness coefficient, |
| $f(\theta)$ | factor for bed slope effect (as a function of Shields parameter), |
| $h_0$ | zero-order solution of the water depth, |
| $g$ | the acceleration of gravity, |
| $u_0$ | zero-order solution of the main flow velocity, |
| $L_a(a/h, C, Z_R) = \frac{\gamma_2+\delta_2}{\gamma_0}$ | dimensionless length scale of convection of suspended sediment concentration, |
| $W$ | cross-sectional width, |
| $\gamma_0, \gamma_2, \delta_2$ | coefficients, and |
| $\theta$ | Shields parameter, |
| $w_s$ | fall velocity. |

Two other important parameters present in every linear analysis are the wavenumber $k_r$ and the damping coefficient $k_i$, the value of which determines the behaviour of the system. The characteristic polynomial he derived is

$$(1-X)\Lambda i x^3 + \left[1 + \Lambda(1-X)(\frac{1}{K} - \frac{b-3}{2})\right] x^2 + \left[\frac{b-3}{2} - (1+\Lambda)\frac{1-X}{K} i\right] x - \frac{1-X}{K} = 0 \quad (2.4)$$

where $X$ is the fraction of total load which is modelled as suspended load, and

$$x = k\lambda_w \quad (2.5)$$

$$k = k_r + ik_i \quad (2.6)$$

$$K = \lambda_s/\lambda_w \quad (2.7)$$

$$\Lambda = \lambda_c/\lambda_w. \quad (2.8)$$

Using a degree of non-linearity equal to 5 ($b = 5$), and a ratio of $\Lambda = 1.6$, the wavenumber and the damping of the solutions are shown in Figure 2.1, for various fractions of suspended load to total sediment load. It is clear that for cases where a large part of the total load is transported as suspended sediment, both modes of sediment transport should be modelled.

It is important to highlight that Talmon (1992) neglected both dispersion and diffusion of suspended sediment in his analysis.

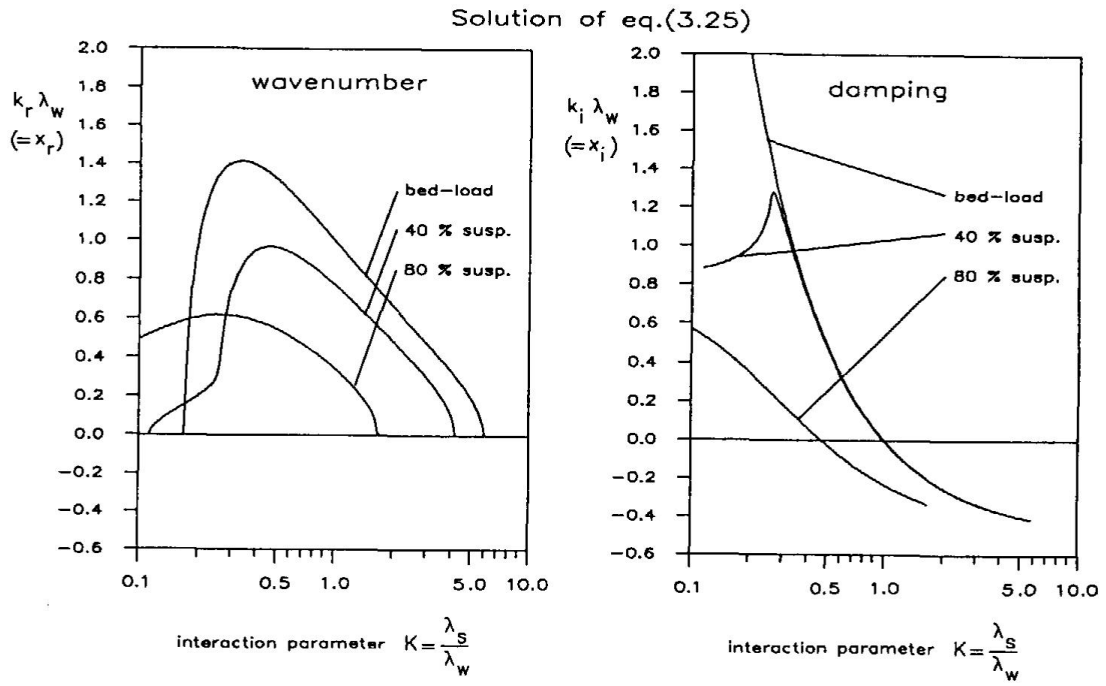


Figure 2.1: Wavenumber and damping with $b = 5$, $\Lambda = 1.6$; (Talmon, 1992).

## 2.2 Influence of secondary flow and diffusion on the suspended sediment concentration field

Z. B. Wang (1989) performed an order of magnitude analysis in the 3D convection-diffusion equation of suspended sediment, in order to identify the relative importance of secondary flow and diffusion for the concentration field. In order to identify the influence of the secondary flow, two convective terms were compared, one in the main and the other one in the secondary flow direction. The first is proven to be much larger than the second. The same conclusion is drawn, when the convective term in the secondary flow direction is compared with the diffusive term in the same direction. The influence of both secondary flow and diffusion on the suspended sediment concentration field can be considered minor. Still, according to Z. B. Wang (1989), the same conclusion is not valid regarding the influence of the processes on the suspended sediment transport. The change on its magnitude is insignificant but not the change on its direction. Reason is the influence that this deviation has in morphological predictions.

# Chapter 3

# Applicability of Van Rijn formulas in river bends using Delft3D

The combination of depth-averaged modelling, using Delft3D in a river bend context, and the sediment transport formulas of Van Rijn can lead to 'strange', unrealistic morphological predictions. The present research is trying to identify the cause of the problem by deconstructing the relevant processes. It is acknowledged, with the help of a real case study in Rio Atrato, Colombia, that suspended sediment transport modelling in a depth-averaged context is to be blamed and not the Van Rijn's formulations, as similar unrealistic behaviour is acknowledged by using a different sediment transport formula in a way that bed load and suspended load transport are explicitly defined. The axi-symmetric solution in cases with suspended sediment load in river bends is now relevant to be investigated. The analysis shows that the magnitude of bed load transport and the diffusive transport in the cross-stream direction of suspended sediment further influence the axi-symmetric solution in comparison to the case without suspended load (assuming that the influence of secondary flow on the suspended sediment is neglected or modelled along with the diffusion). Two more test cases are used, a part of the Rio Atrato, and a hypothetical single bend, both run for sufficient time, approaching the equilibrium solution. Depth-averaged simulations are compared to 3D simulations using the same base settings, and it is shown that the contribution of the horizontal diffusion to the solution can be striking. It is suggested, for morphological predictions in river bends when including suspended sediment load and using the present depth-averaged version of Delft3D, not to depend on the default values for the horizontal diffusion coefficient that is provided by the model, and potentially use a larger spiral flow intensity calibration coefficient than in the case without suspended sediment load (for a detailed explanation of the parameters reference is made to Appendix A.) The latter is an immediate result of the fact that even negative values for the diffusion coefficient can

be required in river bends, if it is to represent both dispersion and diffusion of suspended sediment. This suggestion is disconnected from the physical meaning of the equations, but it is shown to be the only alternative without modifying the current implementation of the numerical model. Still, further investigation is advised, on whether it is acceptable. Finally, it is concluded that it is relevant to investigate the influence of explicitly modelling dispersive transport of suspended sediment in Delft3D (at present it is assumed to be implicitly accounted for along with diffusion), which is also the subject of Chapter 4.

## 3.1 Methodology and results

### 3.1.1 Van Rijn's formulas in river bends using Delft3D

With the morphological model of Melman (2011) as a starting point, it is evident that there is a 'strange' behaviour of Delft3D, in a depth-averaged river bend context, when using the sediment transport formulas of Van Rijn. On the contrary, when two different sediment transport 'predictors' are applied in the same model, the formulas of Engelund and Hansen (1967) and Meyer-Peter and Müller (1948), the results are much more realistic (see Figure 1.1). A major difference between the Van Rijn's formulas and the other two, is that only the first ones explicitly distinguish suspended from bed load sediment transport. As a result, it was realised that it should be investigated if the solution is substantially influenced by modelling bed load and suspended load separately. A scenario based on the case of Rio Atrato is designed where the Van Rijn (1984a, 1984b, 1984c) formulas are partially applied, ignoring the suspended load transport (application only of the bed load formula). The model settings are included in Appendix B. As it is shown in Figure 3.1, the results are now similar to those when the other two sediment transport 'predictors' were applied. The unrealistic predictions are related to suspended sediment transport modelling using the Van Rijn formulations.

Still, it is not known whether the problem is related to this part of the sediment capacity formulations or if in general the way suspended sediment is modelled is to be blamed. For the next test cases, the predicted magnitudes of bed and suspended load are disconnected from measurements, and are modified in order to identify their influence. A second set of simulations, applying the sediment transport formula of Engelund and Hansen (1967), where the total load predicted by the formula is divided into suspended load and bed load at fixed percentages ($X$ representing the fraction of total load that is modelled as suspended load), shows the same unrealistic behaviour (Figure 3.2). The influence of suspended sediment is more and more striking as the ratio of suspended load to bed load increases.

At this point it is clear that the 'strange' behaviour of Delft3D in a river bend context is not strictly related to the Van Rijn's formulas, but to suspended sediment transport

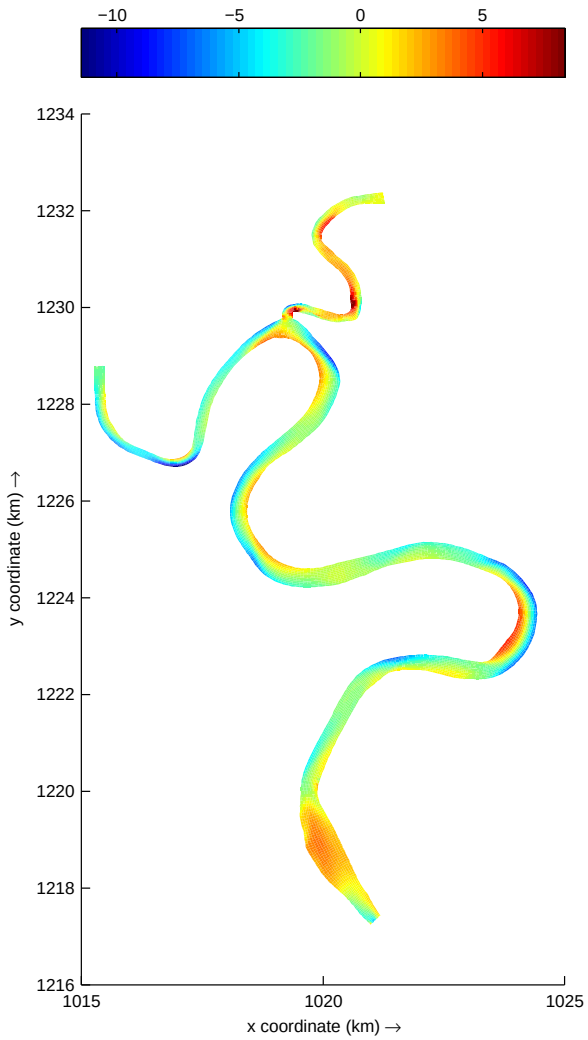


Figure 3.1: Rio Atrato case study run only with bed load using Van Rijn (1984a); bed levels in [m], $t = 100\,\mathrm{yr}$.

modelling. Either the inapplicability of the model, or bad modelling practices with suspended sediment transport could be blamed.

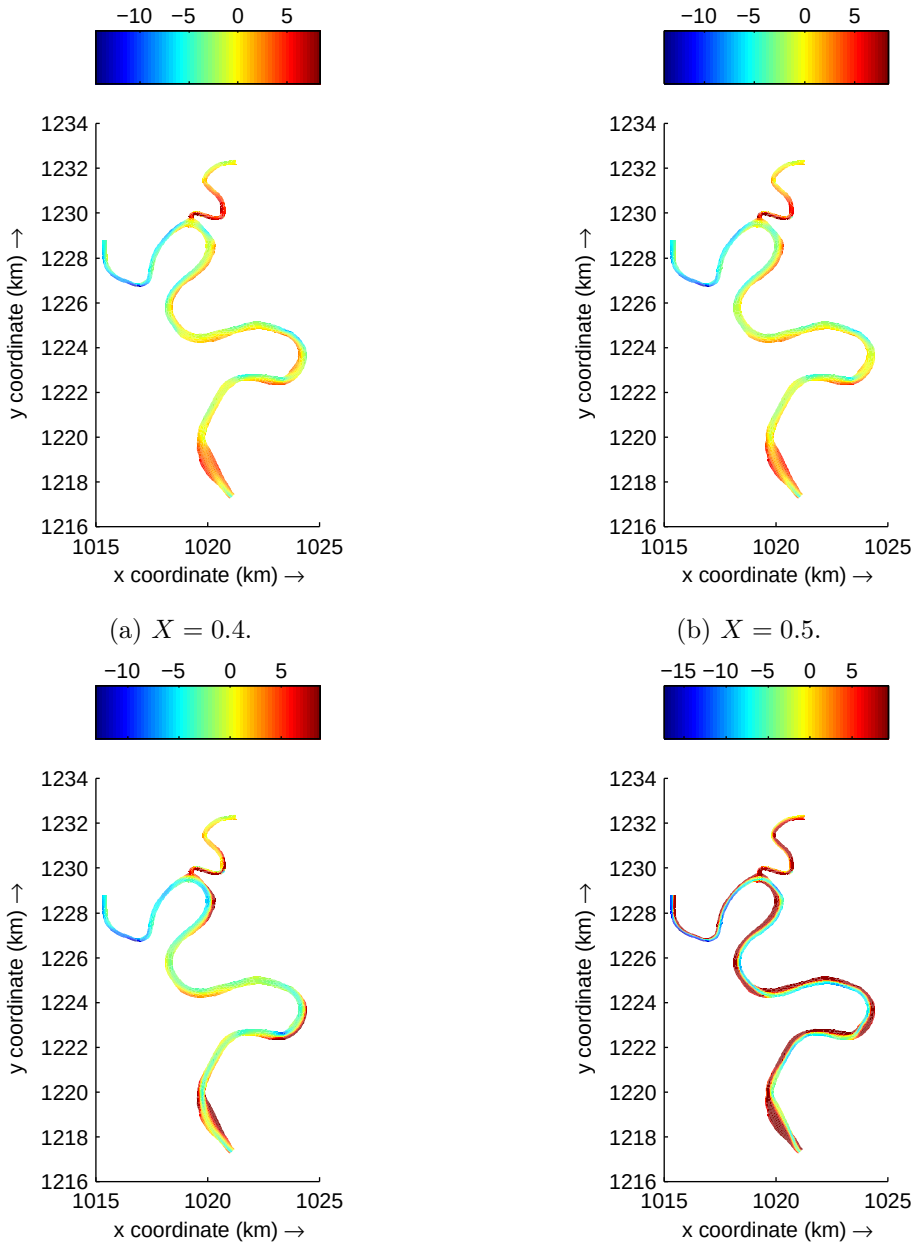


(a) $X = 0.4$.

(b) $X = 0.5$.

(c) $X = 0.6$.

(d) $X = 0.7$.

Figure 3.2: Rio Atrato case study modelling both bed and suspended load using Engelund and Hansen (1967); bed levels in [m], $t = 100\,\text{yr}$.

### 3.1.2 Axi-symmetric solution

Modelling both bed load and suspended sediment transport using Delft3D in a river bend context can lead to unrealistic morphological predictions. Whether this is a result of bad modelling practices or a limitation to the model exists, is still unknown. In order to answer

the above question it would be highly relevant to quantify the influence of suspended sediment transport on the equilibrium solution in river bends. This is possible by means of the axi-symmetric solution, viz. the equilibrium solution for the transverse bed slope in an infinitely long bend with constant curvature. An analysis for deriving a simplified solution in the axi-symmetric region of river bends in cases with suspended sediment transport is performed.

Considering Equation A.28 (see Appendix A), in the fully developed region of a bend with constant curvature, where the depth-averaged velocity coincides with the streamwise direction, we have,

$$\tan a = \frac{S_b^n}{S_b^s} \tag{3.1}$$

where,

| | |
|---|---|
| $a$ | the angle between the bed load transport vector and the depth-averaged flow vector, |
| $S_b^s, S_b^n$ | the bed load transport component in streamwise (only due to the main flow) and cross-stream (only due to secondary flow) direction, respectively, and |
| $s, n$ | the streamwise and cross-stream coordinates, respectively. |

By definition, for the equilibrium solution in the axi-symmetric region all gradients in time and streamwise direction are zero, and Equation A.38 becomes (ignoring the extra terms due to the change from a Cartesian to a curvi-linear coordinate system)

$$\frac{\partial S_b^n}{\partial n} + \frac{\partial S_{sus}^n}{\partial n} = 0. \tag{3.2}$$

with $S_{sus}^n$ the suspended sediment transport component in the cross-stream direction. At the boundaries of the cross-section both the bed load transport vector and the suspended load transport vector normal to the boundaries vanish, or

$$S_b^n|_{n=0} = S_b^n|_{n=W} = 0 \tag{3.3}$$

$$S_{sus}^n|_{n=0} = S_{sus}^n|_{n=W} = 0, \tag{3.4}$$

Solving Equation 3.2, and applying the boundary conditions at one of the boundaries we

have,

$$S_b^n + S_{sus}^n = 0. \tag{3.5}$$

From this point onwards a sediment transport formula of the form $mu^n$ will be assumed, and the suspended sediment load will be assumed to be a fixed percentage of the total load. As a result for the sediment transport capacities it is,

$$S_b^s \sim (1 - X)mU^n \tag{3.6}$$

$$S_{sus}^s = CU \int_a^h f_s f_c \mathrm{d}z \sim XmU^n \tag{3.7}$$

$$S_{sus}^n = CI \int_a^h f_{sec} f_c \mathrm{d}z - \int_a^h \epsilon_{sn} \frac{\partial c}{\partial n} \mathrm{d}z \tag{3.8}$$

where,

| | |
|---|---|
| $a$ | a reference height which divides the two modes of sediment transport in suspended and bed load, |
| $C$ | the depth-averaged suspended sediment concentration, |
| $I$ | the spiral flow intensity (equal to $Uh/R$ in equilibrium with $h$ the water depth, and $R$ the radius of curvature of the streamline), |
| $f_s, f_{sec}, f_c$ | the normalized main flow, secondary flow, and suspended sediment concentration profiles, respectively, |
| $U$ | the depth-averaged flow velocity, |
| $z$ | the vertical coordinate, and |
| $\epsilon_{sn}$ | the horizontal diffusion coefficient in the cross-stream direction. |

Using Equation A.28, Equation 3.1, Equation 3.5, Equation 3.6, Equation 3.7 and, Equation 3.8,

$$\frac{\partial z_b}{\partial n} = \left( \frac{XI \frac{\int_a^h f_{sec} f_c \mathrm{d}z}{\int_a^h f_s f_c \mathrm{d}z}}{U(1 - X)} - \frac{\int_a^h \epsilon_{sn} \frac{\partial c}{\partial n} \mathrm{d}z}{(1 - X)mU^n} + A\frac{h}{R} \right) f(\theta). \tag{3.9}$$

where,

| | |
|---|---|
| $f(\theta)$ | factor for bed slope effect (as a function of Shields parameter), |
| $\frac{\partial z_b}{\partial n}$ | transverse bed slope, and |
| $A$ | coefficient for accounting the effect of spiral flow to the direction of bed shear stress. |

If we were to neglect suspended sediment transport, the solution of the transverse bed slope would converge to

$$\frac{\partial z_b}{\partial n}|_{onlybedload} = A\frac{h}{R}f(\theta). \tag{3.10}$$

A comparison of Equation 3.9 and Equation 3.10 can quantify the influence of suspended sediment transport for the equilibrium solution in the axi-symmetric region. In particular, the first two terms on the right hand side of Equation 3.9 represent the contribution of suspended sediment to the axi-symmetric solution of the bed slope, while the third term represents the contribution of bed load. In any case, the influence of a transverse bed slope is not taken into account for the suspended sediment transport, which is known to be inaccurate (Talmon, 1992).

**Neglecting secondary flow influence**

The analysis neglecting the secondary flow influence in the direction of suspended sediment transport is relevant because it is closely related to the current implementation in Delft3D. In this case one could assume that suspended sediment might affect the wave length and damping of the solution due to the linear behaviour of the river bed, but not the axi-symmetric solution. This assumption would be based on the hypothesis that suspended sediment transport would follow the direction of the water flow velocity field, and as a result there would be no transport component in the direction of the transverse slope. The following reasoning is proven to be wrong. After rearranging, and neglecting the first term on the right hand side of Equation 3.9 we get

$$\frac{\partial z_b}{\partial n} = \left( A\frac{h}{R} - \frac{\int_a^h \epsilon_{sn}\frac{\partial c}{\partial n}\mathrm{d}z}{S_b^s} \right) f(\theta). \tag{3.11}$$

Taking the ratio of Equation 3.11 to Equation 3.10,

$$\left(\frac{\partial z_b}{\partial n}\right)' = \left( 1 - \frac{\int_a^h \epsilon_{sn}\frac{\partial c}{\partial n}\mathrm{d}z}{S_b^s}\frac{R}{Ah} \right) \frac{\partial z_b}{\partial n} \tag{3.12}$$

where the prime stands for the transverse bed slope when suspended sediment transport is

included. We can see that the $\tan a$ term may be very small (small angle), but it scales with $R/(Ah)$, which is relatively large. The influence of suspended sediment on the transverse slope can be important. It could even be possible that the axi-symmetric solution changes sign leading to bars in outer bend regions and to pools in the inner bend regions.

**Accounting for secondary-flow influence along with diffusion**

The axi-symmetric solution for the cases where dispersion of suspended sediment is either explicitly or implicitly modelled has to be the same. This effectively means that the horizontal diffusion coefficient shall be calibrated in such a way that the first two terms on the right-hand side of Equation 3.9 (explicit modelling) are equal to the second term of Equation 3.11 (implicit modelling). According to this principle, we have

$$\left(-\frac{\int_a^h \epsilon_{sn}\frac{\partial c}{\partial n}\mathrm{d}z}{(1-X)mU^n}\right)' = \frac{XI\frac{\int_a^h f_{sec}f_c\mathrm{d}z}{\int_a^h f_s f_c\mathrm{d}z}}{U(1-X)} - \frac{\int_a^h \epsilon_{sn}\frac{\partial c}{\partial n}\mathrm{d}z}{(1-X)mU^n} \tag{3.13}$$

and assuming the same concentration (small influence of dispersion and diffusion of suspended sediment on the concentration field) and velocity field in both instances

$$\epsilon'_{sn} = \epsilon_{sn} - \frac{XImU^{n-1}}{\int_a^h \frac{\partial c}{\partial n}\mathrm{d}z}\frac{\int_a^h f_{sec}f_c\mathrm{d}z}{\int_a^h f_s f_c\mathrm{d}z} \tag{3.14}$$

Equation 3.14 shows the appropriate value for the diffusion coefficient for which the axi-symmetric solution is reached. This is roughly the value that should be applied in the axi-symmetric region of river bends when using Delft3D, assuming that it represents both dispersion and diffusion of suspended sediment. The first term on the right-hand side accounts for the actual diffusion coefficient of suspended sediment, which is a positive parameter. The second term on the same side shows the contribution of dispersion and its sign depends on that of spiral flow intensity and of the depth-averaged transverse gradient of suspended sediment concentration. Assuming that a constant value for $\epsilon'_{sn}$ is appropriate for representing both effects (something that is known to be inaccurate), negative values could be possible, depending on this second term. Of course, this can be the case only in a river bend context, as in straight reaches a negative diffusion coefficient is unrealistic. Under the present implementation in Delft3D, only a positive constant coefficient can be applied by the user.

A similar analysis based on the principle that the axi-symmetric solution shall be the same, regardless of modelling dispersion explicitly or implicitly, can lead tentatively to the

conclusion that the need for a negative value for the diffusion coefficient can be eliminated by calibrating either the spiral flow intensity or the fraction of total load that is considered as suspended load ($X$; see Equation 3.9). The complications of the first option are the unknown influence of secondary flow on the wave length and the damping of the solution in a river bend, and the fact that the physical meaning of secondary flow is disconnected from its value. Moreover, modifying the spiral-flow intensity could lead to unrealistic hydrodynamic results. On the other hand, the second option is immediately rejected, based on the linear analysis made by Talmon (1992).

### 3.1.3 Test cases with the help of the axi-symmetric solution

The analysis indicated that problems related with suspended sediment modelling using Delft3D can be related to the way secondary flow influence on suspended sediment is treated in a depth-averaged context. It has been realised that the influence of the horizontal diffusion has to be investigated with more test cases. It is possible that even negative values for the horizontal diffusion coefficient are needed in river bends. In that case an unrealistic value for the spiral flow intensity could overcome this demand. Two models are used, a hypothetical bend and a part of the Rio Atrato by Melman (2011).

#### Hypothetical bend

The axi-symmetric solution is hardly reached in the Rio Atrato model. As a result, a hypothetical, simplified, single-bend model domain with constant width and curvature is used where an axi-symmetric region exists, for testing the analysis. The settings of the simulation are included in Appendix B for reference.

Initially three simulations are designed, in order to investigate if the unrealistic predictions with suspended sediment transport modelling using Delft3D are related to the depth-averaging; one 3D simulation in 30 equidistant layers, one 2D depth-averaged simulation with the same base settings, and one 2D depth-averaged simulation without suspended sediment transport. The default value of the diffusion coefficient in Delft3D is applied where relevant (the same value as used by Melman, equal to $\epsilon_s = 10\,\mathrm{m^2\,s^{-1}}$), along with the Van Rijn (1984a, 1984b, 1984c) formulas (the suspended sediment transport part is ignored in the last case.) The equilibrium water depths at the centerline and near the banks of the model domain are plotted, after being normalized with the depth at the entrance of the bend (Figure 3.3). The results can be explained by means of the axi-symmetric solution. It is evident that using the same horizontal diffusion coefficient in the 3D and in the 2DH simulation with suspended sediment can be the source of unrealistic predictions. If the value of the diffusion coefficient would approach zero, the solutions of the two depth-averaged cases (with and without suspended sediment) are expected to be the same

in the axi-symmetric region. Moreover, a negative value of the coefficient is needed for approaching the axi-symmetric solution of the 3D simulation.

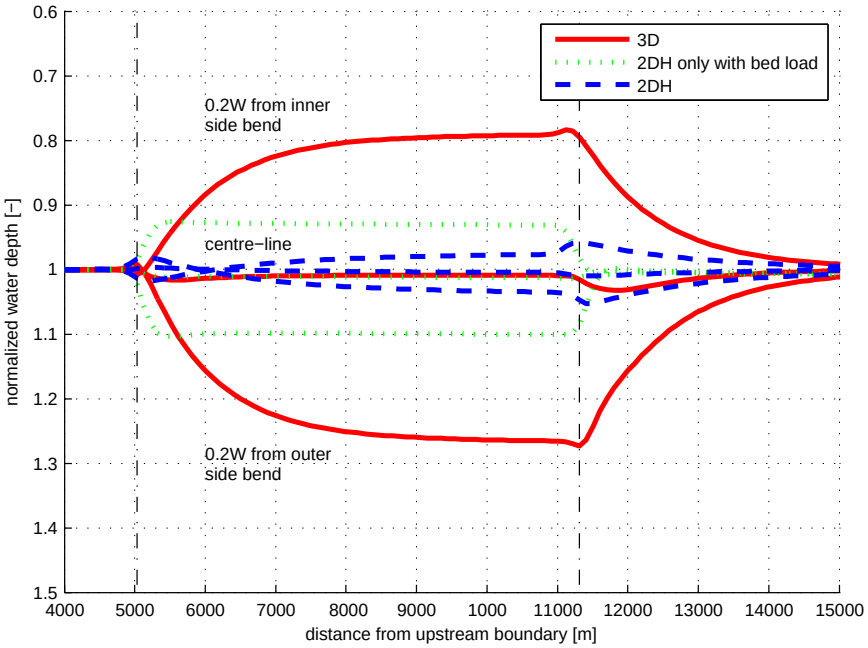


Figure 3.3: Hypothetical bend; normalized equilibrium water depth without calibration, $R = 2000\,\mathrm{m}$.

The influence of a small value for the diffusion coefficient is explored with a depth-averaged simulation. Once again, the normalized water depths from 3 different simulations are plotted (Figure 3.4a.) Two of them are the same as before (3D and 2DH without suspended sediment), and the third is a new 2DH simulation where the horizontal diffusion coefficient is equal to zero. The results show that the axi-symmetric solution coincides with the one without suspended sediment modelling as expected. Both the wave length and the damping of the solution are greatly affected by using horizontal diffusion as a calibrating parameter for approaching the axi-symmetric solution.

It is examined whether it is possible to calibrate the model in such a way that the axi-symmetric solution from the 3D simulation is reached. In order to avoid using a negative value for the diffusion coefficient, only the spiral flow intensity is modified (increased with a factor equal to 3.5). This leads the solution to approach the one from the 3D simulation (Figure 3.4b), with the wave length and the damping to be similar.

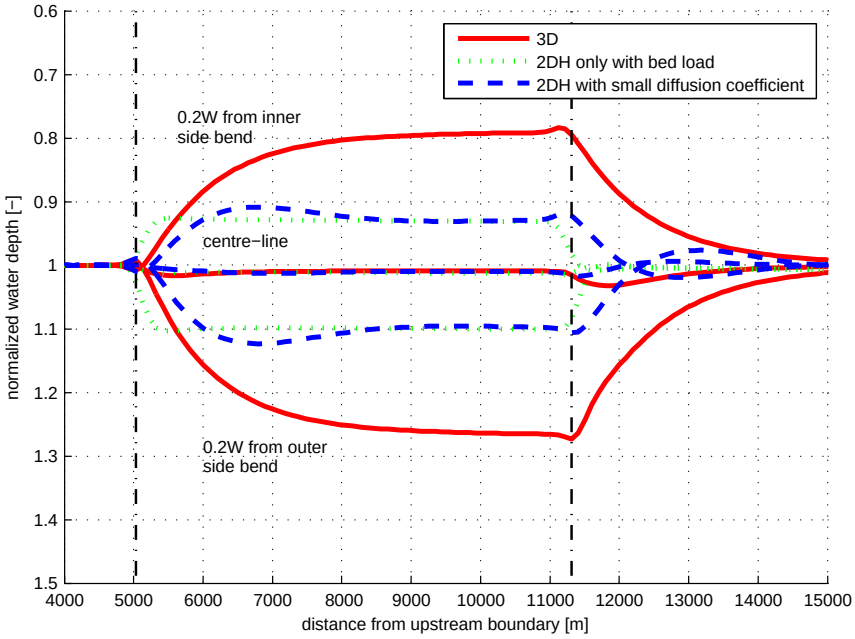


(a) Zero horizontal diffusion of suspended sediment.

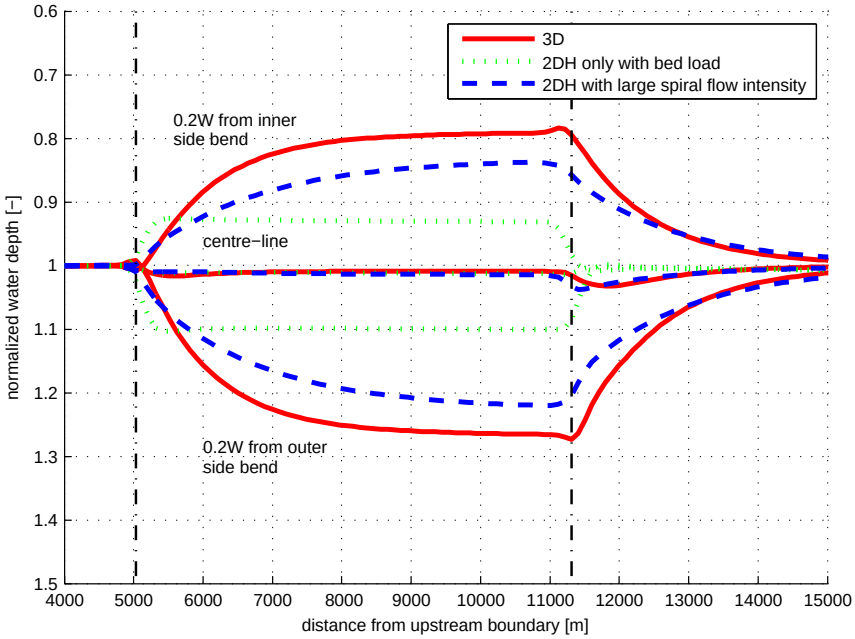


(b) Large spiral flow intensity.

Figure 3.4: Hypothetical bend; influence of calibration on the normalized equilibrium water depth, $R = 2000\,\mathrm{m}$.

### Part of Rio Atrato

Due to the large computational demand of the model developed by Melman (2011), a part of the total domain is used. The model is split in such a way that the relevant information is still included. The sediment transport formulas of Van Rijn (1984a, 1984b, 1984c) are used, in 3D and 2DH simulations. Suspended sediment transport modelling is included in all the simulations except a depth-averaged one, which is used for comparison. The calibrated values for the magnitudes of bed load and suspended load by Melman (2011) are used when relevant.

The concentration field could provide an indication for the need for calibration. If the depth-averaged concentration is larger in the inner-bend regions compared to the outer-bend regions, a diffusive flux of suspended sediment concentration towards the outer bank is expected. This net effect of suspended sediment transport is the opposite of what Talmon (1992) observed physically and a negative value for the diffusion coefficient could be demanded. As it is shown in Figure 3.5 this is the case. Either a small value for the diffusion coefficient has to be used or a calibration coefficient for the spiral flow intensity larger than unity.

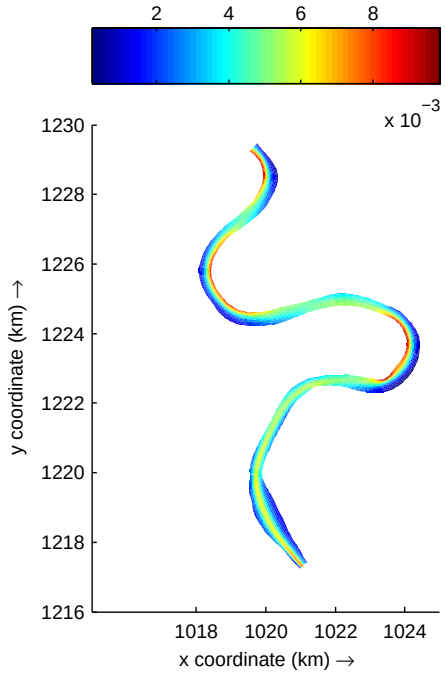


Figure 3.5: Part of Rio Atrato; concentration of suspended sediment in $[kg/m^3]$, $t = 100\,\mathrm{yr}$.

It is investigated whether a more proper solution can be achieved by influencing either of the two. Similarly to the previous test cases, a 3D simulation for a part of the Rio Atrato domain is compared to a calibrated depth-averaged simulation. Both calibrating the diffusion coefficient and the spiral flow intensity is tested (increased with a factor equal to 1.8). The results show that the solution can be improved (Figure 3.6).

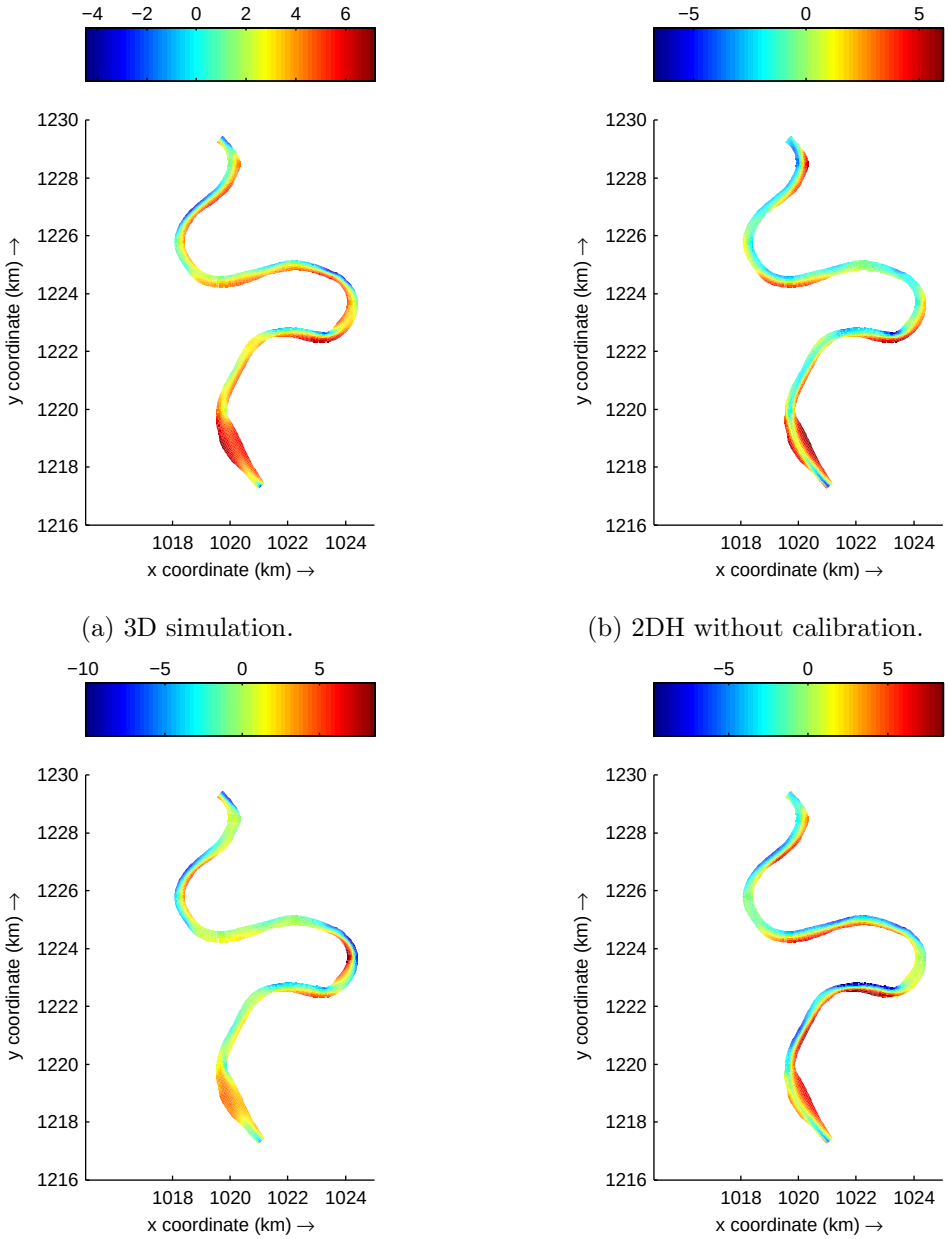


(a) 3D simulation.

(b) 2DH without calibration.

(c) 2DH with small diffusion coefficient.

(d) 2DH with calibrated spiral flow intensity.

Figure 3.6: Part of Rio Atrato; influence of calibration on bed levels in [m], $t = 100\,\mathrm{yr}$.

## 3.2 Discussion

It has been realised that suspended sediment transport modelling in a river bend context, using the 2D depth-averaged version of Delft3D, should be applied with extreme caution. The horizontal diffusion coefficient is considered a calibration parameter and as a result it should be treated as such. The modeller could also use a calibration factor for the spiral flow intensity larger than unity, assuming that the wave length and the damping of the solution will be affected only to a small extent. The numerical experiments indicate that both are strongly influenced by the diffusion coefficient but not by the spiral flow intensity. At least, this is the case when the secondary flow influence is taken into account for the direction of bed load sediment but not for the suspended load sediment. A new linear analysis including suspended sediment transport is needed in order to further support the indication as in the existing one by Talmon (1992), the effects of both secondary flow and diffusive transport are neglected.

The calibration that is proposed is for enhancing the accuracy of morphological predictions in river bends by depth-averaged models that either neglect or implicitly model the influence of secondary flow on the suspended sediment. Especially when influencing the spiral flow intensity, an unrealistic direction for the bed load sediment transport is used in order to correct the erroneous direction of the suspended sediment load transport. Moreover, the influence of the spiral flow intensity on the water flow velocity field has not been examined. It is totally uncertain whether the model could be calibrated in such a way when for example bifurcations are present. In order to overcome this problem, to minimize the need for calibration of the model, and to avoid disconnecting the parameters from their physical meaning, the possibility of explicitly modelling the influence of secondary flow on the suspended sediment transport has to be investigated. This is the study subject of Chapter 4.

The whole analysis is based on a simplified axi-symmetric solution. In the Rio Atrato, hardly any axi-symmetric region exists. The influence of other important elements of the model is unknown. Galapatti's formulations that determine the adaptation length and time scales of the suspended sediment transport model applied in Delft3D and the influence of the horizontal diffusion in streamwise direction can also be relevant.

# Chapter 4

# Modelling secondary flow influence on suspended sediment transport

Incorporating the influence of secondary flow on depth-averaged modelling including suspended sediment transport by using a constant diffusion coefficient as a calibrating parameter is problematic. Not only the value of the diffusion coefficient has to change in space and time, but also negative values may be required. The possibility of explicitly modelling the influence of dispersive transport of suspended sediment in Delft3D is investigated. An analysis based on the axi-symmetric solution in river bends including suspended sediment is used in order to identify potential problems of such an implementation. It is realized that if the influence of a transverse slope on the suspended sediment transport is neglected, the axi-symmetric solution can approach infinity. Moreover, it is expected that the solution is sensitive to the information lost by the depth-averaging, viz. the secondary-flow velocity and suspended sediment concentration field. With the above limitations in mind, a depth-integrated suspended sediment model is designed. It is based on Delft3D, with the addition of the depth-averaged expressions for the effects of secondary flow by using analytical similarity profiles of sediment concentration (Rouse) and secondary flow (Kalkwijk & Booij, 1986). The newly derived model is implemented in the code of Delft3D and is used in several test cases. Its performance is promising. The results in many cases closely approach solutions from 3D simulations also using Delft3D with the same base settings, without need for calibration. On the contrary, in situations where the spiral flow intensity is large (see for definition Chapter 3), and the banks of the rivers are modelled as vertical walls, the newly derived model fails. The analysis indicates the reason to be the inaccurate calculation of the spiral flow intensity near the boundaries, in those situations. In order to test this hypothesis the depth-integrated secondary flow model is combined with another modified version of Delft3D, initially adapted by Ottevanger (2013), where a distribution function

is incorporated. After the new implementation, the solution near the banks is improved considerably. It is concluded that in the current version of Delft3D, the incorporation of the effect is valuable, but limits the applicability of the model. A better description of the secondary-flow field is important, especially near the model boundaries. Moreover, further research is advised regarding the high uncertainly of the influence of a sloping bed on the transverse component of suspended sediment transport, a process that could be dominant.

## 4.1 Methodology

### 4.1.1 Importance of dispersion due to the influence on the transverse bed slope in the axi-symmetric solution

We assume that the diffusive transport component of suspended sediment is an order of magnitude smaller than the transport component due to secondary flow (without formal proof). Ignoring the diffusive transport from Equation 3.9, we get

$$\frac{\partial z_b}{\partial n} = \left( \frac{XI \frac{\int_a^h f_{sec} f_c \mathrm{d}z}{\int_a^h f_s f_c \mathrm{d}z}}{U(1-X)} + A\frac{h}{R} \right) f(\theta). \tag{4.1}$$

and after taking the ratio to Equation 3.10 and performing a scale comparison ($z = h\sigma$), it is

$$\frac{\text{Suspended sediment contribution}}{\text{Bed load contribution}} = \frac{X}{(1-X)A} \frac{\int_0^1 f_{sec} f_c \mathrm{d}\sigma}{\int_0^1 f_s f_c \mathrm{d}\sigma}. \tag{4.2}$$

It is expected that $\int_0^1 f_{sec} f_c \mathrm{d}\sigma / \int_0^1 f_s f_c \mathrm{d}\sigma > 1$ if we consider the profile shapes. The magnitude of $X/((1-X)A)$ depends in the value of $X$. For large $X$ or more generally for large suspended sediment transport magnitude in comparison with bed load transport magnitude the contribution of suspended sediment transport is significant. In the special case that $X$ approaches 1, the ratio is,

$$\lim_{X \to 1^-} \frac{X}{(1-X)A} = +\infty. \tag{4.3}$$

The above indicates instability of the solution for $X \approx 1$. Figure 4.1 shows the contribution of the suspended load with respect to the bed load in establishing the transverse bed slope, for varying the ratio of suspended load to the total load ($X$). This contribution is further

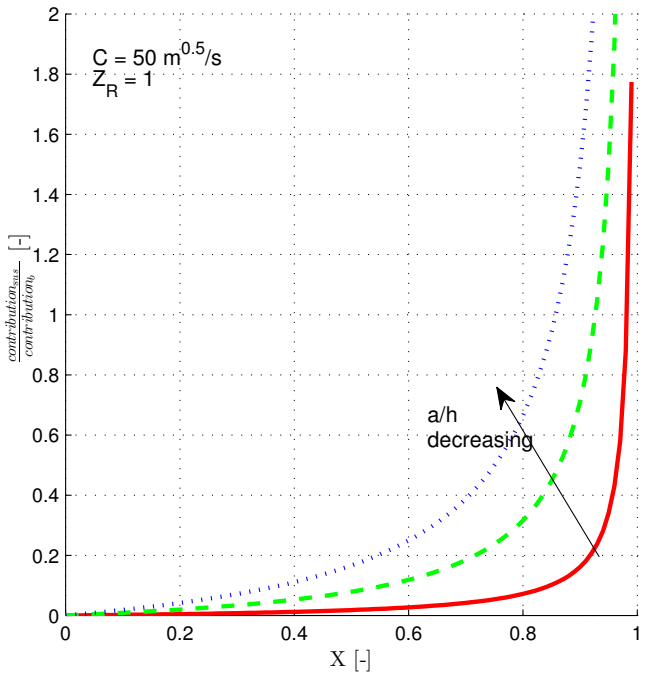


Figure 4.1: Contribution of suspended sediment to the axi-symmetric solution in relation with the bed load transport.

influenced by the ratio of the reference height to the water depth ($a/h$), by the Chézy smoothness coefficient ($C$), and by the Rouse number ($Z_R$). It has to be realized, for example, that when the ratio of the contributions is one, the slope is expected to double compared to the solution without suspended load. This is physically translated by the fact that the transverse slope is stabilized when the bed slope is large enough for cancelling out the transverse bed load sediment transport component. The bed slope only affects the bed load, and without it there could not be such a stabilizing process. A question-observation is posed:

1. Does a transverse bed slope influence the suspended sediment transport load?

Answering this question is not straightforward. By means of the 'unphysical' case that $X \approx 1$ the answer to the first question at least for the mathematical part, would be yes. This point could be explained even better by considering the case where the cross-stream suspended sediment transport component has larger magnitude than the bed load transport magnitude. In that case, even if the transverse bed slope would lead the total bed load to be transported in the transverse direction, this would not be enough for cancelling the cross-stream suspended load vector. In this context, it would be more reasonable to

assume that suspended load would lead to a transverse bed load transport component which does not depend on the magnitude of the bed load itself. Physically, it can intuitively be understood that the transverse bed slope not only influences the bed load transport, but also a part of the suspended sediment transport near the bed. For example, if it would be possible to follow the trajectory of a single grain in time, we could see that although it may belong to suspended load transport, occasionally it can come in contact with the bed, at time scales much smaller that the ones that we consider. Experimental proof to the above was found by Talmon (1992) by means of bed levelling experiments.

**Importance of errors in the profiles**

Three semi-empirical profiles are used, which can lead to inaccurate solutions. Only the accuracy of the secondary-flow profile and the suspended sediment concentration profile will be examined, as the accuracy of the main-flow profile will be considered satisfactory.

The secondary-flow profile is considered to be linear in the area of our interest (mild curvature limit), and the error due to this approximation is expected to be large only near the horizontal boundaries. Assuming that the reference height is above the boundary layer of the secondary flow, this error can be considered negligible, and the accuracy of the approximation depends on the spiral flow intensity $I$ (see previous chapter for definition). Attention has to be paid to the importance of the error, something that is justified with the following reasoning:

- Let us assume that we start with a zero transverse slope on a flat bed and that there is an initial error in the calculation of $I$, with $\delta > 1$ and $\delta = I_{error}|_{t=0}/I_{real}$. That would lead to a larger slope than the correct one. How much larger depends on the difference between actual and calculated value of the spiral flow intensity.

- This higher slope will increase $I$ as $I \approx Uh/R$ in the outer-bank region and decrease $I$ in the inner-bank region.

- The new value of spiral flow intensity will further increase the transverse slope at the outer bank and decrease it at the inner bank. This process will continue until stabilization of the system.

The above reasoning is weak because it is based on a steady-state solution (with predefined bathymetry), when at the same time it includes changes in time. A better explanation, even still not a solid proof, if portrayed into mathematical expressions, could read (assuming R constant)

$$
\begin{aligned}
I_{real}|_{t=\Delta t} &\approx I_{real}|_0 + I'_{real}|_0 \Delta t \\
&\approx I_{real}|_0 + \frac{1}{R}\left(h\frac{\partial U}{\partial t}|_{real} + U\frac{\partial h}{\partial t}|_{real}\right)\Delta t \\
I_{error}|_{t=\Delta t} &\approx I_{error}|_0 + I'_{error}|_0 \Delta t \\
&\approx \delta I_{real}|_0 + \frac{1}{R}\left(h\frac{\partial U}{\partial t}|_{error} + U\frac{\partial h}{\partial t}|_{error}\right)\Delta t.
\end{aligned}
$$

Taking their difference it can be noticed that the error increases over time for the outer bank and decreases for the inner bank (assuming that for larger $I$ the change in velocity and height over the same time period is higher.)

It has to be noted that the secondary-flow profile should flatten near the banks, until it would vanish completely. As it is implemented in Delft3D, this is not the case for rivers with vertical walls at the sides. This leads to an overprediction of $I$ near the boundaries. A distribution function over the width which would force a vertical secondary-flow profile near the banks can decrease the error in that case.

$$\frac{\partial z_b}{\partial n}|_{error} > error|0\frac{\partial z_b}{\partial n} \qquad \text{Outer bank region} \tag{4.4}$$

$$\frac{\partial z_b}{\partial n}|_{error} < error|0\frac{\partial z_b}{\partial n} \qquad \text{Inner bank region} \tag{4.5}$$

Realising that a higher slope is expected when suspended load is included, the same error in the spiral flow intensity will lead to larger absolute height differences.

The error due to the approximation of the suspended sediment profile is also important because for example a steeper profile than the correct one will underestimate the term $< f_s f_c >$ ($<>$ denote depth-averaging), but overestimate the term $< f_{sec} f_c >$. Taking the ratio of the two, the error can be large.

### 4.1.2 Sediment transport model

#### Suspended sediment concentration

The convection-diffusion equation is transformed from a Cartesian to a curvilinear coordinate system with the help of metric coefficients. For clarity, the expressions herein will be presented in a Cartesian system, where one axis will be along the streamwise direction and the other along the cross-stream direction. Moreover, extra terms that are included in Delft3D to represent processes that are not directly relevant to the implementation will be

ignored. The 3D mass balance equation for suspended sediment concentration reads

$$\frac{\partial c}{\partial t} + \frac{\partial uc}{\partial s} + \frac{\partial vc}{\partial n} + \frac{\partial \omega c}{\partial z} = \frac{\partial}{\partial s}\left(\epsilon_s \frac{\partial c}{\partial s}\right) + \frac{\partial}{\partial n}\left(\epsilon_n \frac{\partial c}{\partial n}\right) + \frac{\partial}{\partial z}\left(\epsilon_z \frac{\partial c}{\partial z}\right) \tag{4.6}$$

where

| | |
|---|---|
| $c$ | suspended sediment concentration, |
| $\omega$ | relative velocity in vertical direction (relation of water flow velocity field and fall velocity of sediment), |
| $\epsilon_s, \epsilon_n$ | horizontal diffusion coefficients in the streamwise and cross-stream direction respectively, and |
| $\epsilon_z$ | vertical diffusion coefficient. |

The velocities and the concentration can be normalized with their depth-averaged values,

$$u = U_{tot} f_s cos(\phi) + I_s f_{sec} \tag{4.7}$$

$$v = U_{tot} f_s sin(\phi) + I_n f_{sec} \tag{4.8}$$

$$c = C f_c \tag{4.9}$$

with $C$ the depth-averaged suspended sediment concentration, $U_{tot}$ the depth-averaged velocity, and $\phi$ the angle between $s$ and the secondary-flow direction. An extra definition is needed for the implementation in Delft3D where

$$C_s = \frac{\int_a^h u_{tot} c \mathrm{d}z}{h U_{tot}} \tag{4.10}$$

where $C_s$ is the depth-averaged concentration as defined in the model. Moreover,

$$I_s = -sin(\phi) I \tag{4.11}$$

$$I_n = cos(\phi) I \tag{4.12}$$

Equation 4.7 and Equation 4.8 can be further simplified into,

$$u = Uf_s + I_s f_{sec} \tag{4.13}$$

$$v = Vf_s + I_n f_{sec} \tag{4.14}$$

Substituting the above definitions in Equation 4.6 and then depth-averaging with the help of the kinematic boundary conditions (no flux of sediment across the water surface and one of the near-bed boundary conditions as defined in the Appendix A), and assuming that $h - a \approx h$ and that the horizontal diffusion coefficient is isotropic ($\epsilon_s = \epsilon_n = \epsilon_H$), the 2DH mass-balance equation for suspended sediment concentration is derived (Equation 4.15),

$$\frac{\partial hC}{\partial t} + \frac{\partial}{\partial s}\left(hUC_s + \boxed{hI_sC\frac{\int_a^h f_{sec}f_c\mathrm{d}z}{\int_a^h f_s f_c\mathrm{d}z}}\right) + \frac{\partial}{\partial n}\left(hVC_s + \boxed{hI_nC\frac{\int_a^h f_{sec}f_c\mathrm{d}z}{\int_a^h f_s f_c\mathrm{d}z}}\right) = \frac{\partial}{\partial s}\left(h\epsilon_H\frac{\partial C_s}{\partial s}\right) + \frac{\partial}{\partial n}\left(h\epsilon_H\frac{\partial C_s}{\partial n}\right) + E - D \tag{4.15}$$

with $a$ a reference height inside the water column above which sediment transport is considered as suspended load. In order to solve this equation, the dispersion terms due to secondary flow have to be computed. For the main-flow velocity the logarithmic velocity profile is applied as described in Kalkwijk and De Vriend (1980), the secondary-flow profile is based on a linear approximation by Kalkwijk and Booij (1986), and the concentration profile that is used is the so-called Rouse profile. The Rouse profile has to be further elaborated as it is normalized with the near-bed sediment concentration and not the depth-averaged concentration. Finally, the profiles are given by

$$f_s = 1 + \frac{\sqrt{g}}{\kappa C} + \frac{\sqrt{g}}{\kappa C}\ln\left(1 + \frac{z-h}{h}\right) \tag{4.16}$$

$$f_{sec} = \frac{2}{\kappa^2}m_b\left(\frac{1}{2} + \frac{z-h}{h}\right) \tag{4.17}$$

$$m_b = \frac{m_1}{2} - \frac{\sqrt{g}}{\kappa C}m_1 \tag{4.18}$$

$$m_1 \approx 3 \tag{4.19}$$

$$f_c = \frac{h-\alpha}{\int_a^h f_{Rouse}\mathrm{d}z} \tag{4.20}$$

$$f_{Rouse} = \left[\frac{\frac{h-z}{z}}{\frac{h-\alpha}{\alpha}}\right]^{Z_R} \tag{4.21}$$

$$Z_R = \frac{w_s}{\kappa u_*} \tag{4.22}$$

with $\kappa$ the von Karman coefficient.

### Suspended load transport direction

Suspended sediment load is defined as,

$$S_{sus} = \int_a^h c u_{tot}\mathrm{d}z \tag{4.23}$$

After Reynolds time-averaging, and splitting the flux into the $s$ and $n$ directions, it is,

$$S^s_{sus} = \int_a^h cu\mathrm{d}z - \int_a^h \epsilon_H \frac{\partial c}{\partial s} \tag{4.24}$$

$$S^n_{sus} = \int_a^h cv\mathrm{d}z - \int_a^h \epsilon_H \frac{\partial c}{\partial n} \tag{4.25}$$

Using Equation 4.13, Equation 4.14, and Equation 4.9,

$$S^s_{sus} = UC_s h + \boxed{ChI_s \frac{\int_a^h f_{sec} f_c \mathrm{d}z}{\int_a^h f_s f_c \mathrm{d}z}} - \int_a^h \epsilon_H \frac{\partial c}{\partial s} \tag{4.26}$$

$$S^n_{sus} = VC_s h + \boxed{ChI_n \frac{\int_a^h f_{sec} f_c \mathrm{d}z}{\int_a^h f_s f_c \mathrm{d}z}} - \int_a^h \epsilon_H \frac{\partial c}{\partial n} \tag{4.27}$$

### Implementation

In reality, the secondary flow velocities in the vertical plane vanish near the banks. When these boundaries are modelled as vertical walls, Delft3D overpredicts the spiral flow intensity. A function that forces its value to approach zero near the boundaries is necessary in those situations. This is possible by means of a distribution function. Such an option is not included by default in Delft3D, but it does in a modified version of the software by Ottevanger

(2013). As a result the depth-integrated sediment transport model was implemented both in the default version of Delft3D and the modified one.

Some important remarks regarding the implementation are:

- the spiral flow intensity $I$ is always taken explicitly,
- in order to reduce the simulation time, the influence of secondary flow on the suspended sediment is ignored when $I \leq 1 \times 10^{-5}\,\mathrm{m\,s^{-1}}$. In this way the dispersion is ignored in the straight sections of the domains.
- In order to identify the main and the secondary flow directions, it is assumed that the first direction is the one where the depth-averaged velocity is the largest. This assumption is particularly important for modelling of bifurcations.
- Spiral flow intensity is calculated differently between the adapted version by Ottevanger (2013) and the default one. The purpose of the research is to explore only the influence of the distribution function and not of a different value of the spiral flow intensity. As a result it was assumed that the simulations with the adapted version were 'uncalibrated', but in fact the spiral flow intensity was modified in order to be the same at the centerline of the simulations as the one computed by the default version of Delft3D (with using a calibration coefficient different than unity).
- A new subroutine is included in Delft3D that computes the term $(\frac{\int_a^h f_{sec} f_c \mathrm{d}z}{\int_a^h f_s f_c \mathrm{d}z})$. The integrals are computed with the trapezoidal rule in 20 equidistant layers.
- Delft3D uses the same routine for modelling all the conservative quantities. The influence of secondary flow differs between them due to their different vertical profiles. As a result modelling the influence of dispersion is possible only for the suspended sediment transport (and for example not for salinity or temperature). The initial routine in Delft3D was split into two versions, one for modelling suspended sediment concentration, and the other one for all the other conservative constituents.
- The influence of secondary flow on the suspended sediment transport direction has been implemented in the routine that computes bed level changes.

It is not claimed that the present implementation is the optimum one. The purpose of the research was not to design an efficient algorithm but to acknowledge the importance of physical processes.

## 4.2 Numerical experiments

The implementation in Delft3D is tested with several sets of cases. The main purpose of the model is to be able to predict morphological equilibria, and reactions to changes in the physical conditions at the correct time scales. In the frame of the numerical experiments that are performed only the first one is examined. Preferably, the performance would be assessed in comparison with field measurements, flume experiments, and inefficient but accurate numerical models (DNS, LES) with capabilities for morphological predictions. The availability of data and resources dictated the comparison with flume experiments only, and 3D morphological simulations based on the shallow-water equations (SWE). Essentially, the vertical flow structure is captured in 3D models. As a result, it would be reasonable to compare the depth-averaged version of the model with the actual 3D version of it. Ideally, the same picture would be captured by the two, especially regarding morphological predictions, without need for calibration of the newly introduced factors.

It is important to understand the simplifications and assumptions after depth-averaging. These are:

- The influence of secondary flow on the velocity field is parameterized,
- The bed shear stress depends on the depth-averaged velocity,
- The direction of bed load transport is based on the influence of the parameterized secondary flow,
- The suspended sediment load is modelled as defined by Galappatti (1983), and as a result the adaptation time and length scales are approximated, and
- The newly introduced simplification, where the influence of the secondary flow on the convection of sediment concentration and the direction of suspended sediment transport are based on semi-empirical parameterizations of the secondary flow and the sediment concentration profiles.

Three different types of numerical experiments are conducted. A hypothetical set of single-bend models, with the same flow and sediment properties belongs to the first type. They are designed in such a way that the ratio of suspended to bed load is large. By decreasing the radius of curvature in the different models, the sensitivity to the spiral flow intensity will be investigated. The only reference for their performance will be 3D simulations with the same settings. A dataset from flume experiments conducted by Talmon (1992) with suspended sediment transport is also used in order to asses the performance of the modified model. Suspended load transport and bed load transport are approximately of

the same order of magnitude, and the modification in Delft3D is not expected to be crucial (see Figure 4.1). The final set is based on the model by Melman (2011) in the Rio Atrato, Colombia, which is a typical example where unrealistic predictions were modelled when including suspended sediment load. In the present chapter only a part of the numerical experiments is presented (the rest is included in Appendix B), necessary for reaching the conclusions.

### 4.2.1 Hypothetical bend experiments

Many parameters influence the performance of the depth-averaged numerical model. Regarding the modifications applied in Delft3D, and assuming that the depth-averaged concentration is calculated accurately with Galapatti's convection-diffusion equation, the most important parameter is expected to be the accuracy of the secondary-flow model and the value of the spiral flow intensity. Delft3D overpredicts the secondary flow near the side boundaries when they are modelled as vertical walls. The ratio of $h/R$ is a crucial factor for the performance of the model, not only due to the limitation in the validity of the secondary-flow model, but mainly because of the overprediction of the spiral flow intensity near the boundaries. That is the reason for choosing to modify the radius of curvature between different cases. The experiments will show how important the error can be, and whether a distribution function can correct it.

The performance of the depth-integrated model is assessed by using results from 3D simulations with the same base settings. The domain consists of two straight sections with one circular bend of 180 degrees. The Van Rijn (1984a, 1984b, 1984c) sediment transport formula is used. The normalized water depths near the banks and the centerline of the model are plotted (normalized with the depth at the entrance of the bend). The implementation is more accurate for the model with the larger radius of curvature (Figure 4.2).

It is hypothesized that the reason is the inaccurate representation of the spiral flow intensity near the boundaries. The version of the model where a distribution function is incorporated is used in order to verify the hypothesis. Still, due to the different methods for calculating the spiral flow intensity, different values of it were computed even at the centreline, and a variable calibration factor was applied for minimizing that difference. As already stated, the model was calibrated, not with a criterion of a better accuracy but of the desired value of the spiral flow intensity at the centerline (the case with the distribution function has to have the same spiral flow intensity at the centerline with the default version of Delft3D). For small curvatures (or relatively small spiral flow intensity) the transverse slope is predicted more accurately without the distribution function except in the region near the banks (Figure 4.3a), whereas the solution is greatly improved for larger curvatures (Figure 4.3b).

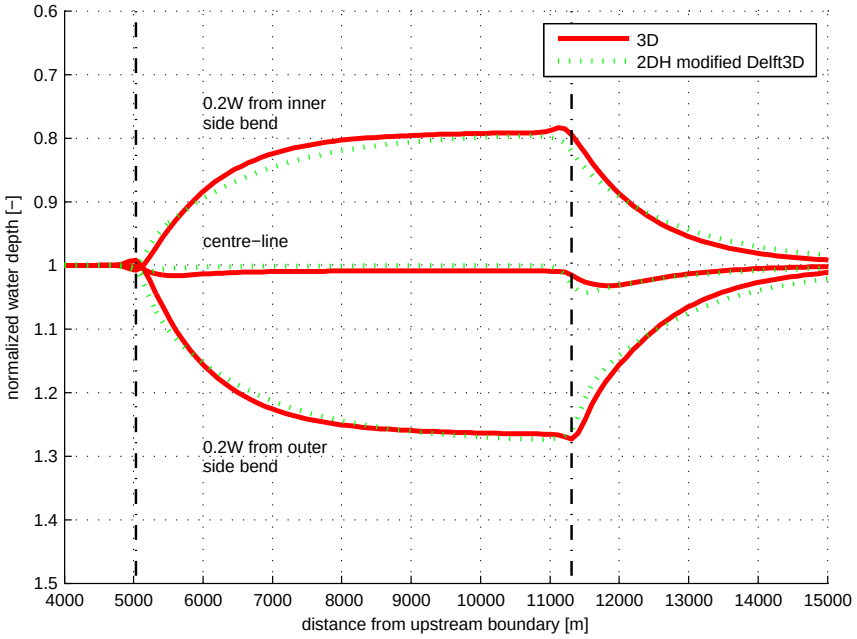


(a) $R = 2000\,\mathrm{m}$.

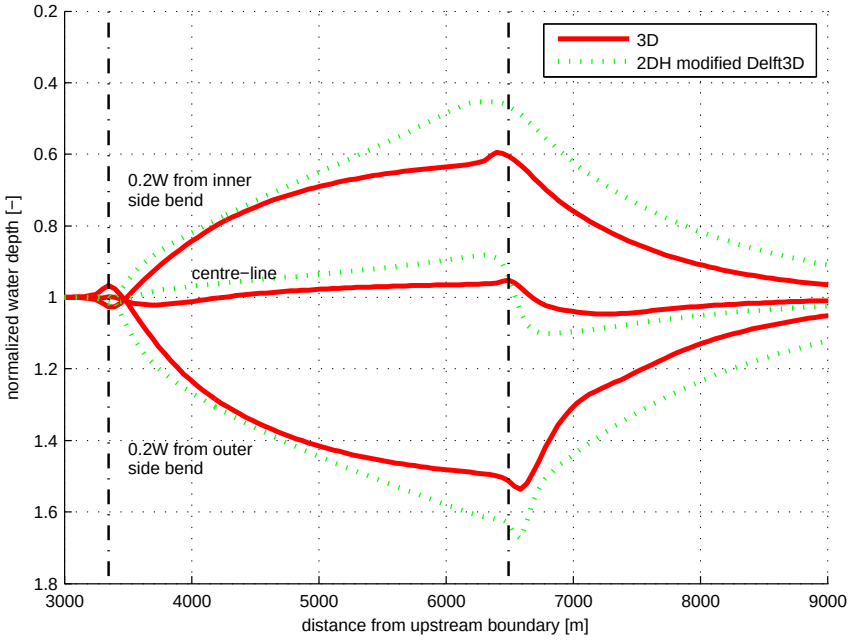


(b) $R = 1000\,\mathrm{m}$.

Figure 4.2: Hypothetical-bend run with the modified version of Delft3D; equilibrium streamwise normalized water depths near the banks and the centerline.

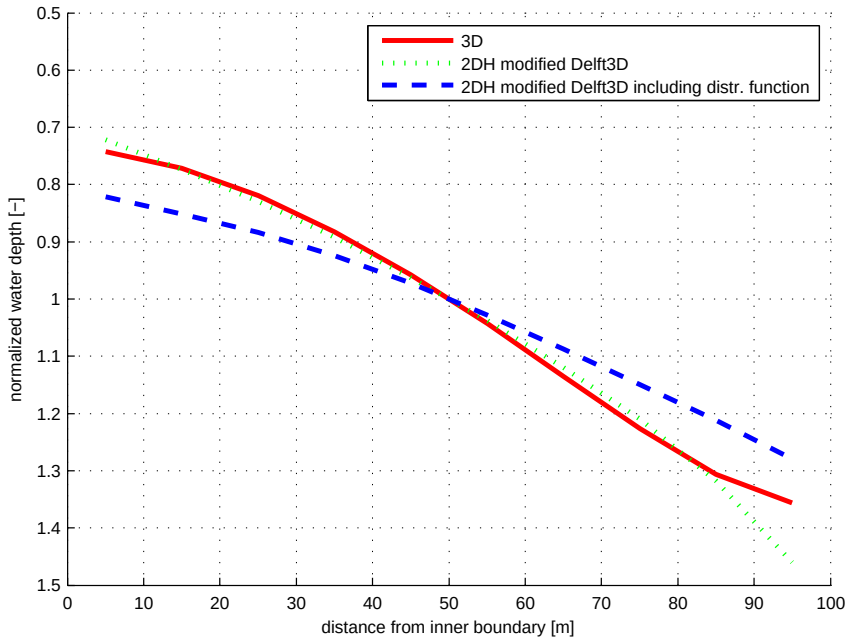


(a) $R = 2000\,\mathrm{m}$.

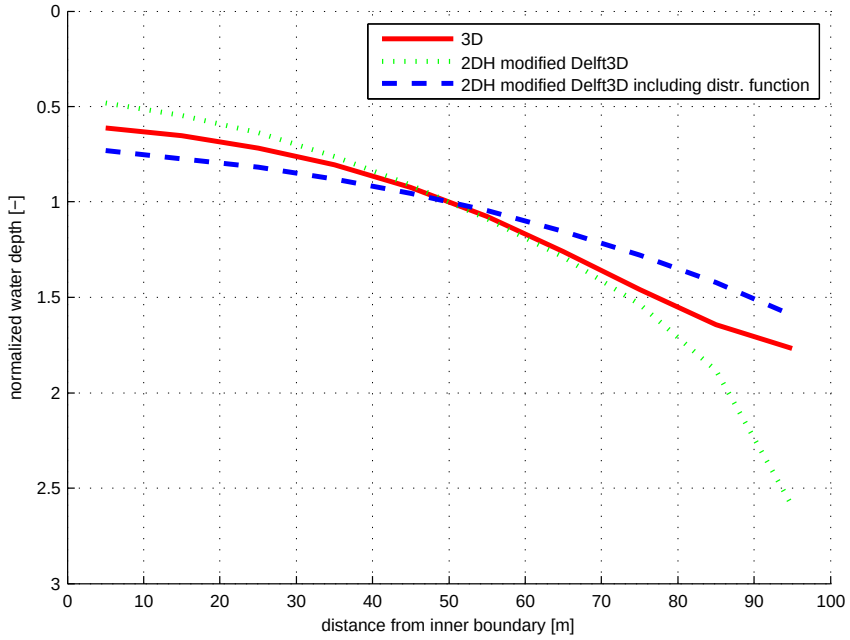


(b) $R = 1000\,\mathrm{m}$.

Figure 4.3: Hypothetical-bend run with the modified version of Delft3D; axi-symmetric solution.

### 4.2.2 Rio Atrato case study

The morphological model by Melman (2011) that pointed out the necessity of this study is used. It would be interesting to test if explicit modelling of the influence of the secondary flow on the suspended sediment using Delft3D improves the solution, without the calibration method discussed in the previous chapter. Once again, a part of the model domain is used (see Chapter 3), along with the sediment transport formulas of Van Rijn (1985). The large curvatures of many bends in the model and the banks which are modelled as vertical walls demand the use of the distribution function. The spiral flow intensity is again influenced in order to match the value given by the default version of Delft3D. The performance of the 'improved' code is explored with the help of a 3D simulation with the same base settings.

The results are shown in Figure 4.4. Qualitatively, the solution is greatly improved (see previous chapter). Still, considerably larger water depths are predicted compared to the 3D simulations.

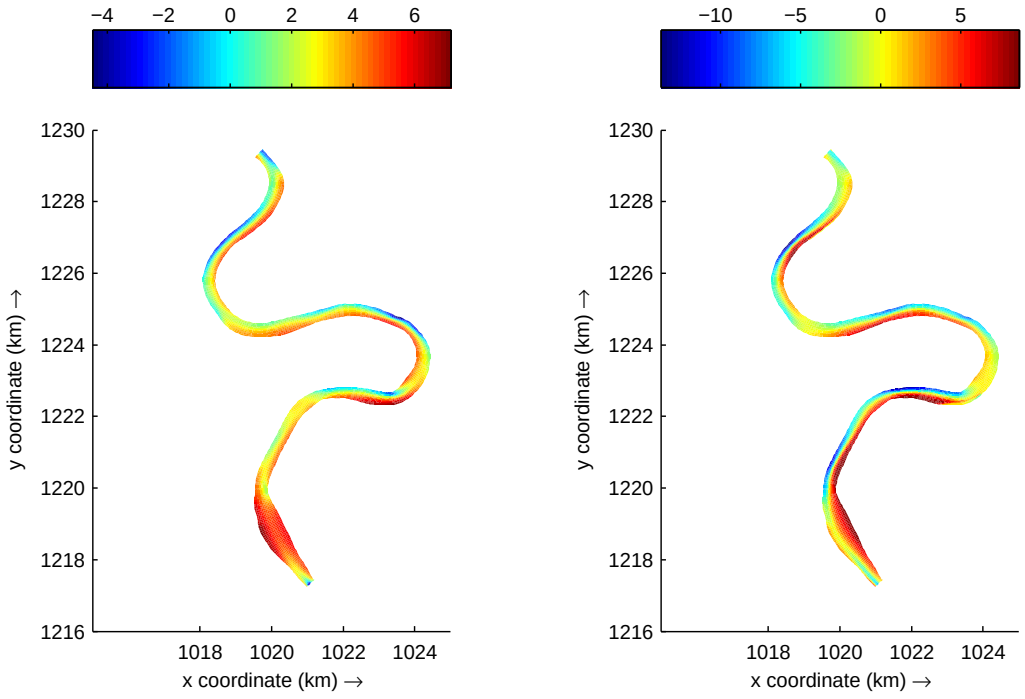


(a) 3D simulation.

(b) 2DH simulation with modified version including distribution function.

Figure 4.4: Part of the Rio Atrato case study run with the modified version of Delft3D; bed levels in [m], $t = 100\,\mathrm{yr}$.

## 4.3 Discussion

Incorporating the influence of secondary flow on the suspended sediment in depth-averaged morphological models is highly valuable. It avoids the need for calibration that would lead to disconnecting parameters from their physical meaning. Still, further research is necessary, especially regarding the influence of a transverse bed slope on the suspended sediment transport. With the present implementation, this effect is accounted for by assuming a greater influence of the bed slope on the bed load sediment transport, which seems physically unrealistic.

The performance of the model depends greatly on the accuracy of calculating the secondary flow. A distribution function is necessary in situations with large spiral flow intensities, when the boundaries are modelled as vertical walls. Of course this demand is not absent in the situation where only the bed load sediment is modelled, but it is hidden behind the fact that larger transverse slopes are expected in situations with suspended sediment load. For example, if in the physical system suspended sediment load occurs but we neglect it, we may finally arrive at a correct transverse slope by overestimating the secondary flow. This is not the case when including both modes of transport and when the overestimation becomes problematic.

The implementation proposed is not the optimum one. It was not designed with a criterion of efficiency, but to investigate the possibilities of modelling suspended sediment transport using Delft3D. One main reason, for example, is the need for numerically computing integrals, which results in slower morphological computations than by the actual depth-averaged version of Delft3D (including suspended sediment modelling). Either analytical or approximate solutions for the profiles could be derived or existing models for which solutions exist could potentially be used.

# Chapter 5

# Conclusions and recommendations

The present research identifies that problematic morphological predictions using the depth-averaged version of Delft3D and applying the sediment transport formulas of Van Rijn (1984a, 1984b, 1984c) are connected to suspended sediment transport modelling. In particular, the solution of the depth-averaged model is sensitive to the value of the horizontal diffusion coefficient, and becomes unrealistic, under two conditions. The first condition is that the influence of secondary flow on the suspended sediment transport has to be neglected, or has to be implicitly modelled (assuming that the dispersive stresses are included in the diffusive turbulent stresses by treating the horizontal diffusion coefficient as a calibration parameter). The second condition is that the bed load transport has to be sufficiently small.

Furthermore it can be necessary, in morphological modelling of river bends using Delft3D and including suspended sediment, to use a negative value for the diffusion coefficient as it accounts for the influence of both dispersive and diffusive stresses. In straight reaches, a negative value of the diffusion coefficient has no physical meaning. As a result a constant user-defined value (as implemented in Delft3D) is not sufficient in such cases. In order to overcome this demand, it seems possible to use an unrealistically large value for the spiral flow intensity.

An alternative to the above calibration principles would be to explicitly model the influence of secondary flow on the suspended sediment. Incorporating this process in Delft3D can greatly improve the solution, although there are some limitations. Firstly, the secondary-flow intensity and the depth-averaged sediment concentration have to be computed accurately enough. This is of essence not only at the centerline of the model domains, but also near the banks. The above condition is becoming more and more important as the curvature of the models increases. Models with relatively large curvatures, where the lateral boundaries are modelled as vertical walls, demand the use of a distribution function of the spiral flow intensity along the width. Moreover, there is large uncertainty on the influence of a sloping bed on the suspended sediment transport in the transverse

direction.

Using the above conclusions as a starting point the following is recommended:

- Suspended sediment transport modelling, using the depth-averaged version of Delft3D in a river bend context, should be applied with caution. The horizontal diffusion coefficient is considered a calibration coefficient and shall be treated as such. Reliance on the default values provided by the software is not recommended. Gradients of the concentration field shall be identified, and with the help of the axi-symmetric solution the models should be calibrated accordingly.

- The inclusion in Delft3D of the effect of secondary flow on the direction of suspended sediment transport, along with the possibility of using a distribution function (along the width) for the spiral flow intensity, would be beneficial.

- The influence of spiral flow intensity and diffusion of suspended sediment on the wave length and the damping of the solution in river bends shall be identified by means of a new linear analysis. In this way the possibility of using the secondary flow as a calibration parameter could be examined more extensively.

- Further research is demanded regarding the influence of the bed slope on the direction of suspended sediment transport. Until now, only the influence on the bed load has been modelled. In simulations with suspended sediment transport, a larger influence on the bed load could be used in order to implicitly take this effect into account. This is not considered to be physically realistic, and a different approach is recommended to be identified.

# Bibliography


Ananyan, A. K. (1965, orig. publ. in Russian 1957). *Fluid flow in bends of conduits* (I. P. for Scientific Translations Ltd., Ed.). Jerusalem.

Bagnold, R. A. (1941). *The physics of blown sand and desert dunes*. London: Methuen.

Bagnold, R. A. (1973). The nature of saltation and of 'bed-load' transport in water. *Proceedings of the Royal Society of London. A. Mathematical and Physical Sciences*, *332*(1591), 473–504. doi:10.1098/rspa.1973.0038

Blanckaert, K. (2002). *Flow and turbulence in sharp open-channel bends* (Ph. D. thesis, École polytechnique fédérale de Lausanne). Retrieved February 19, 2014, from http://infoscience.epfl.ch/record/161943/files/2010-752-Blanckaert-Flow_separation_in_sharp_meander_bends.pdf

Blanckaert, K. (2009). Saturation of curvature-induced secondary flow, energy losses, and turbulence in sharp open-channel bends: laboratory experiments, analysis, and modeling. *Journal of Geophysical Research: Earth Surface*, *114*(F3). doi:10.1029/2008JF001137

Boussinesq, J. (1868). Mèmoire sur l' influence de frottement dans les mouvements règuliers des fluides; xii- essai sur le mouvement permanent d' un liquide dans un canal horizontal á axe circulaire. *J. de Math. Pures et Appl.* 2ème Série, *Tome XIII*, p.413. Retrieved February 19, 2014, from http://sites.mathdoc.fr/JMPA/PDF/JMPA_1868_2_13_A17_0.pdf

De Vriend, H. J. (1981). *Steady flow in shallow channel bends* (Ph. D. thesis, Delft University of Technology). Retrieved February 19, 2014, from http://repository.tudelft.nl/assets/uuid:d42e1810-6657-4941-9703-a2c08a6550f1/DeVriend1981.pdf

De Vries, M. (1959). *Transients in bed-load-transport (basic considerations)*. Delft Hydraulics Laboratory.

De Vries, M. (1965). *Considerations about non-steady bed-load-transport in open channels*. Delft Hydraulics Laboratory.

De Vries, M. (1993). *Use of models for river problems*. Unesco. Retrieved May 27, 2014, from http://resolver.tudelft.nl/uuid:13b8565a-9b49-4d35-8897-25b430b5a320

Einstein, H. A. (1950). *The bed-load function for sediment transportation in open channel flows*. US Department of Agriculture. Retrieved March 3, 2014, from http://www.vliz.be/imisdocs/publications/75/247675.pdf

Engelund, F. & Hansen, E. (1967). *A monograph on sediment transport in alluvial streams*. Teknisk forlag Copenhagen. Retrieved March 3, 2014, from http://repository.tudelft.nl/assets/uuid:81101b08-04b5-4082-9121-861949c336c9/Engelund_Hansen1967.pdf

Galappatti, R. (1983). *A depth integrated model for suspended transport*. Communications on hydraulics. Delft University of Technology, Department of Civil Engineering. Retrieved March 3, 2014, from http://repository.tudelft.nl/assets/uuid:2cf67a5b-d2c4-4287-8ed2-16f1b27bdbcc/CommHydr8307.pdf

Huang, S., Jia, Y. F., & Wang, S. S. Y. (2006). Numerical modeling of suspended sediment transport in channel bends. *Journal of Hydrodynamics, Ser. B*, *18*(4), 411–417. doi:10.1016/S1001-6058(06)60113-3

Jansen, P. P., Van Bendegom, L., Van den Berg, J., De Vries, M., & Zanen, A. (1979). *Principles of river engineering: the non-tidal alluvial river*. Water Resources Engineering Series. Delftse Uitgevers Maatschappij. Retrieved March 3, 2014, from http://repository.tudelft.nl/assets/uuid:15e01b6c-57b7-4229-8dda-9eefaf979443/2443-1003.pdf

Kalkwijk, J. P. T. & Booij, R. (1986). Adaptation of secondary flow in nearly-horizontal flow. *Journal of Hydraulic Research*, *24*(1), 19–37. doi:10.1080/00221688609499330. eprint: http://dx.doi.org/10.1080/00221688609499330

Kalkwijk, J. P. T. & De Vriend, H. J. (1980). Computation of the flow in shallow river bends. *Journal of Hydraulic Research*, *18*(4), 327–342. doi:10.1080/00221688009499539. eprint: http://www.tandfonline.com/doi/pdf/10.1080/00221688009499539

Melman, F. (2011). *Navigability at an unstable bifurcation - the montaño - murindo bifurcation of the atrato river in colombia.*

Meyer-Peter, E. & Müller, R. (1948). Formulas for bed-load transport. In *Proceedings of the 2nd meeting of the international association for hydraulic structures research* (pp. 39–64). Stockholm. Retrieved May 27, 2014, from http://repository.tudelft.nl/assets/uuid:4fda9b61-be28-4703-ab06-43cdc2a21bd7/Meyer-PeterMuller1948.pdf

Mosselman, E. (2005). *Basic equations for sediment transport in cfd for fluvial morphodynamics, from computational fluid dynamics: applications in environmental hydraulics* (P. D. Bates, S. N. Lane, & R. I. Ferguson, Eds.). Wiley.

Olesen, K. W. (1987). *Bed topography in shallow river bends* (Ph. D. thesis, Delft University of Technology). Retrieved February 19, 2014, from http://repository.tudelft.nl/assets/uuid:e9b7082e-76dc-407d-a334-3d9e471d5a93/TR%20DISS%201566(1).PDF

Ottevanger, W. (2013). *Modelling and parameterizing the hydro- and morphodynamics of curved open channels* (Ph. D. thesis, Delft University of Technology). Retrieved February 19, 2014, from http://repository.tudelft.nl/assets/uuid:9f19d0ea-5d89-4c15-b99d-3fb02fc28eb7/thesis_Ottevanger_W.pdf

Rozovskii, I. L. (1961, orig. publ. in Russian 1957). *Flow of water in bends of open channels* (I. P. for Scientific Translations Ltd., Ed.). Jerusalem.

Shields, A. (1936). *Application of similarity principles and turbulence research to bed-load movement*. Retrieved June 19, 2014, from http://repository.tudelft.nl/assets/uuid:a66ea380-ffa3-449b-b59f-38a35b2c6658/Shields_-_Application_of_Similarity_Principles_and_Turbulence_Research_to_Bed-Load_Movement.pdf

Talmon, A. M. (1992). *Bed topography of river bends with suspended sediment transport* (Ph. D. thesis, Delft University of Technology). Retrieved February 19, 2014, from http://repository.tudelft.nl/assets/uuid:bd4cdc3e-a4f5-4ba9-977a-1fb9a420f0d0/ceg_talmon_19920622.PDF

Van Rijn, L. C. (1984a). Sediment transport, part i: bed load transport. *Journal of Hydraulic Engineering*, *110*(10), 1431–1456. doi:10.1061/(ASCE)0733-9429(1984)110:10(1431). eprint: http://dx.doi.org/10.1061/(ASCE)0733-9429(1984)110:10(1431)

Van Rijn, L. C. (1984b). Sediment transport, part ii: suspended load transport. *Journal of Hydraulic Engineering*, *110*(11), 1613–1641. doi:10.1061/(ASCE)0733-9429(1984)110:11(1613). eprint: http://dx.doi.org/10.1061/(ASCE)0733-9429(1984)110:11(1613)

Van Rijn, L. C. (1984c). Sediment transport, part iii: bed forms and alluvial roughness. *Journal of Hydraulic Engineering*, *110*(12), 1733–1754. doi:10.1061/(ASCE)0733-9429(1984)110:12(1733). eprint: http://dx.doi.org/10.1061/(ASCE)0733-9429(1984)110:12(1733)

Van Rijn, L. C. (1985). *Sediment transport*. Delft hydraulics laboratory. Retrieved March 3, 2014, from http://kennisonline.deltares.nl/product/20024

Wang, Z. B. (1989). *Mathematical modelling of morphological processes in estuaries* (Ph.D thesis, Delft University of Technology). Retrieved February 19, 2014, from http://repository.tudelft.nl/assets/uuid:5fc9bffd-7d91-4d59-afee-9737021a2b0b/ceg_wang_19890302.pdf

Wendt, J. F. (2009). *Computational fluid dynamics* (J. F. Wendt, Ed.). Berlin, Heidelberg: Springer Berlin Heidelberg. doi:10.1007/978-3-540-85056-4

Wu, W. (2007). *Computational river dynamics*. Taylor & Francis. Retrieved from http://books.google.nl/books?id=baIrUy9OdlIC

Wu, W. & Wang, S. S. Y. (2005). Depth-averaged 2-d calculation of flow and sediment transport in curved channels. *International Journal of Sediment Research*, *19*(4),

241–257. Retrieved March 3, 2014, from http://www.cqvip.com/qk/87646x/200404/11509457.html

# Appendix A

# General framework

The fundamental problem a morphologist has to solve is to predict the topographical changes in a given area, in a given time period. A riverbed can be described as a moving container that responds to the imposed forcing and its boundary conditions. The flowing water generates stresses at the bed and acts either as a source or sink of sediment, directly influencing the topography. The river morphologist is particularly interested in examining the responses of the riverbed due to the water flow. Neglecting chemical bonds and reactions, and assuming that water is a continuous Newtonian fluid, these processes can be described, with high accuracy, by applying mass and momentum conservation to the water as a whole, and to each grain individually. This approach in large scale applications is by current means unfeasible. Instead of computing the trajectories of each grain, the sediment movement is treated at a more macroscopic level. The major implication of this approach is that the source of sediment from the bed has to be computed using semi-empirical formulations based on local flow quantities and general characteristics of the soil. At this level, three important elements need to be addressed; movement of water, movement of sediment, and influence on the topography. These conceptual mechanisms interact. Changes in the sediment transport and in the river geometry directly influence water flow. Mathematically, this is translated into a system of coupled partial differential equations. Still, there is the potential of separating the solving procedure of the flow, the sediment transport, and the bed level changes. Two important assumptions need to be made. Sediment transport and water flow are considered a two-phase flow, except if it is assumed that sediment concentration is so low that it does not affect the water density. Moreover, bed level changes are an order of magnitude slower than changes in the flow field. The solving algorithm can now proceed in stages. First the flow field is computed, then the sediment transport, and in the end the bed level changes (Figure A.1).

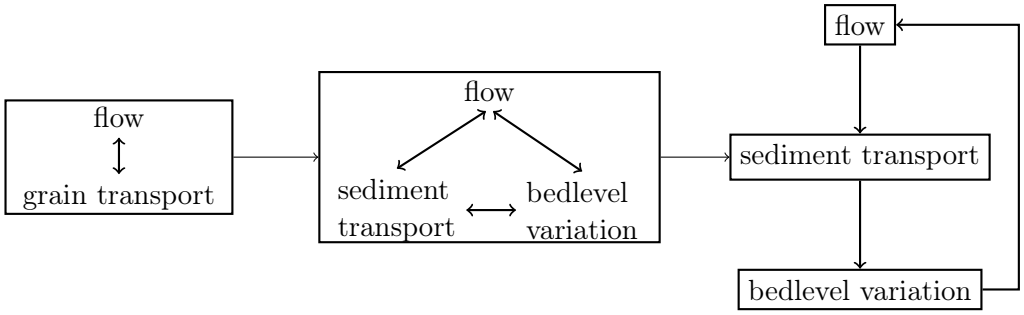


Figure A.1: Simplification of morphological model.

## A.1 Hydrodynamic processes

Fluid motions are accurately described by the Navier-Stokes equations. They are based on the physical concepts of the conservation of mass, momentum, ignoring the theory of relativity, and quantum mechanics processes. Their basic assumption is that fluids are a continuous mean. Using the Einstein's notation they read,

$$\frac{\partial \rho}{\partial t} + \frac{\partial}{\partial x_j}\left[\rho u_j\right] = 0 \tag{A.1}$$

$$\frac{\partial \rho u_i}{\partial t} + \frac{\partial}{\partial x_j}\left[\rho u_i u_j + p\delta_{ij} - \tau_{ij}\right] = 0 \tag{A.2}$$

$$\frac{\partial \rho E}{\partial t} + \frac{\partial}{\partial x_j}\left[\rho u_i E + u_j p + q_j - u_i \tau_{ij}\right] = 0 \tag{A.3}$$

where,

$E$ total energy,
$p$ pressure,
$q_j$ heat,
$t$ time,
$u$ velocity,
$x$ coordinate in the Cartesian system
$\delta_{ij}$ Kronecker delta,
$\rho$ density of the fluid, and
$\tau_{ij}$ stresses.

The problem is ill-defined as there are 5 equations with 6 depended variables, in addition to the shear stresses that have to be determined. The final necessary equation is an equation of state, whereas the shear stresses can be calculated with the help of a viscosity model

(for water usually assuming that it is a Newtonian fluid). The Navier-Stokes equations can only be solved, with direct numerical simulation models (DNS). In order to capture turbulence, fine computational meshes are essential. The number of cells is a function of the Reynolds number ($N \propto Re^{9/4}$), and this makes their implementation in open-channel water flow ($Re \gg 4000$ which is the limit of turbulent flow) practically impossible. This implication drove the development of large-eddy simulation models (LES), proposed by Joseph Smagorinksy. Practically this approach suggests the direct solution only for the larger eddies while modelling parametrically the shear stresses due to the smaller ones. Also this approach demands fine grids and the full parametrical modelling of the turbulent stresses is still relevant. After "Reynolds-averaging" the Navier-Stokes equations, a procedure introduced by Osborne Reynolds, it is possible to ignore the turbulent flow velocity fluctuations while retaining their effects as shear stresses that are calculated by semi-empirical functions. In this way the turbulent stresses are modelled, and even coarser grids are possible to be applied. With this concept, the velocities are decomposed into

$$u_i = \overline{u_i} + u_i' \tag{A.4}$$

where,

$\overline{u}$ Reynolds-averaged velocity,

$u'$ turbulent velocity fluctuation.

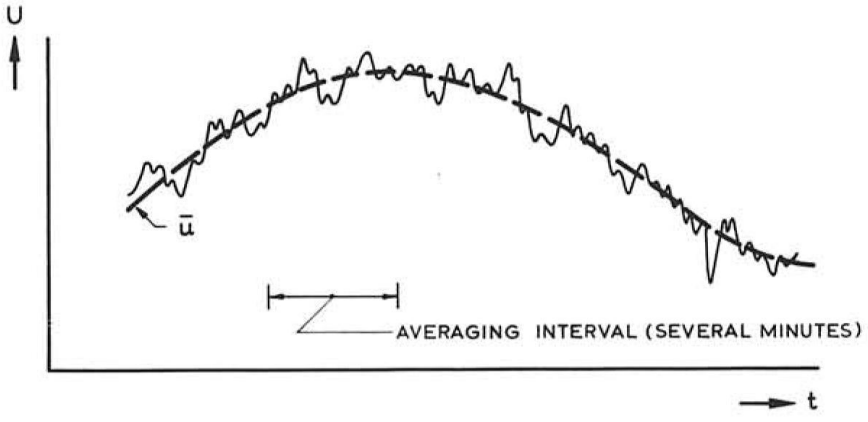


Figure A.2: Time averaging over turbulence; schematic representation (Jansen, Van Bendegom, Van den Berg, De Vries, & Zanen, 1979).

After assuming that the fluid is incompressible in order to decouple the energy balance,

and averaging over a "Reynolds time interval", the Reynolds-averaged mass and momentum Navier-Stokes equations (RANS) read,

$$\frac{\partial}{\partial x_j}\left[\overline{u_j}\right] = 0 \tag{A.5}$$

$$\frac{\partial \overline{u_i}}{\partial t} + \frac{\partial}{\partial x_j}\left[\overline{u_i u_j} + \frac{1}{\rho} p\delta_{ij} - \frac{1}{\rho}\tau_{ji} + \overline{u_i' u_j'}\right] = 0 \tag{A.6}$$

Currently there is an effort of the scientific community towards intermediate models, between RANS and LES.

### A.1.1 From RANS to the 3D shallow-water equations (SWE)

Even for RANS, the grid cell size should be very small and for turbulent flow this is of essence especially near the boundaries. That is because the wall boundary layers become thin, which leads to high velocity gradients, and the diffusive flux is inaccurate on coarse grids. Two types of boundary conditions are defined, one of them designed to overcome this problem. The system of four coupled partial differential equations, three of which of second order, results in relatively slow numerical solutions depending on the requirements for the accuracy (approximation method). The high aspect ratio of grid cell dimensions ($\Delta z \ll \Delta x$) can also be a source of complications. It is not yet practically applicable for large-scale applications in open-channel flow. This is the reason for the use of the shallow-water equations (SWE), both in 2D and 3D models. The main assumptions that are further defined for the simplification are:

- the fluid is incompressible (as already defined for decoupling the energy balance),
- the pressure is hydrostatic,
- deviations in density are much smaller than the actual density ($\Delta\rho \ll \rho$).

From this point onwards we will consider only Newtonian fluids, an assumption that is generally valid for describing the behaviour of water. Moreover the external forces will be separated from the stress tensor. Separating the internal stresses from the external forces, Equation A.5 and Equation A.6 become (henceforth overbar will be omitted i.e. $u_i = \overline{u_i}$),

$$\frac{\partial}{\partial x_j}\left[u_j\right] = 0 \tag{A.7}$$

$$\frac{\partial u_i}{\partial t} + \frac{\partial}{\partial x_j}\left[u_i u_j\right] + \frac{1}{\rho}\frac{\partial p}{\partial x_i} - \frac{1}{\rho}\frac{\partial}{\partial x_i}\left[\tau_{ij}\right] = F_i \tag{A.8}$$

with $F$ the external forcing (Coriolis force etc.), and

$$\tau_{ij} = \rho\nu_t \left( \frac{\partial u_i}{\partial x_j} + \frac{\partial u_j}{\partial x_i} \right) \tag{A.9}$$

where $\nu_t$ is the eddy or turbulent viscosity.

According to the hydrostatic pressure assumption the momentum equation in z direction is simplified into,

$$\frac{\partial p}{\partial z} = -\rho g \tag{A.10}$$

with $g$ the acceleration of gravity. Finally, separating the horizontal eddy viscosity from the vertical one, assuming that the first is much larger than the vertical one due to the different length scales in which they act, including the Coriolis force, the final 3D SWE read ($u_1 \to u$, $u_2 \to v$, $u_3 \to w$, $x_1 \to x$, $x_2 \to y$, $x_3 \to z$),

$$\frac{\partial u}{\partial x} + \frac{\partial v}{\partial y} + \frac{\partial w}{\partial z} = 0 \tag{A.11}$$

$$\frac{\partial u}{\partial t} + \frac{\partial uu}{\partial x} + \frac{\partial uv}{\partial y} + \frac{\partial uw}{\partial z} = \frac{\partial}{\partial x}\left(\nu_h \frac{\partial u}{\partial x}\right) + \frac{\partial}{\partial y}\left(\nu_h \frac{\partial u}{\partial y}\right) + \frac{\partial}{\partial z}\left(\nu_v \frac{\partial u}{\partial z}\right) - g\frac{\partial z_s}{\partial x} - \frac{1}{\rho_0}\frac{\partial p_{atm}}{\partial x} - \frac{g}{\rho_0}\int_z^{z_s} \frac{\partial \rho}{\partial x} \mathrm{d}z + fv \tag{A.12}$$

$$\frac{\partial v}{\partial t} + \frac{\partial vv}{\partial y} + \frac{\partial vv}{\partial y} + \frac{\partial vw}{\partial z} = \frac{\partial}{\partial x}\left(\nu_h \frac{\partial v}{\partial x}\right) + \frac{\partial}{\partial y}\left(\nu_h \frac{\partial v}{\partial y}\right) + \frac{\partial}{\partial z}\left(\nu_v \frac{\partial v}{\partial z}\right) - g\frac{\partial z_s}{\partial y} - \frac{1}{\rho_0}\frac{\partial p_{atm}}{\partial y} - \frac{g}{\rho_0}\int_z^{z_s} \frac{\partial \rho}{\partial y} \mathrm{d}z - fu \tag{A.13}$$

where,

$f$ the Coriolis parameter,
$g$ the acceleration of gravity,
$p_{atm}$ the atmospheric pressure,
$z_s$ the water level,
$\nu_h$ the horizontal eddy viscosity,
$\nu_v$ the vertical eddy viscosity, and
$\rho_0$ the density of the fluid which is updated every new time step from an equation of state.

There are 3 equations with 4 depended variables $(z_s, u, v, w)$, so the system cannot be solved. The solution is possible with the help of the depth-averaged mass-balance equation (Equation A.24), and the definition of the depth-averaged velocities (Equation A.22). The final system results in a turbulence closure model for the calculation of the turbulent viscosities, Equation A.11, Equation A.12, Equation A.13, the depth-averaged continuity equation, the equations that describe the depth-averaged velocities, and an equation of state for taking into account changes in density due to salinity, temperature, and sediment concentration.

### A.1.2 Boundary conditions

The partial differential equations cannot be solved without defining the relevant boundary conditions. They directly influence the solutions of the system and are crucial for a successful computation. At a top level, a distinction is made regarding the nature of the boundary; open or closed. For alluvial channels, the closed boundaries are defined in the interfaces between water and soil, where normal to them a zero transport flux is assumed (impermeable boundary.) It is commonly accepted and verified with experimental results that at closed boundaries the flow velocity is equal to the velocity of the boundary both in normal and in tangential direction (no-slip condition.) The latter condition requires fine vertical computational meshes for resolving the boundary layer and capturing the steep velocity gradients, especially for turbulent flows. As already stated, in order to overcome this demand, the boundary layer is modelled instead of being solved. In our case, we make use of the logarithmic law of the wall for forming the dynamic boundary conditions.

The model boundaries that are not closed are consequently open. For open channel flow, a special type of open-boundary condition that is most commonly used is at the water surface (interface between water and air). Taking the boundary above this interface would require modelling a two-phase flow. Also this boundary is considered 'impermeable', as we assume zero exchange of the fluid with the air. This assumption may seem physically paradoxical, but fits its purpose in combination with the shallow-water equations.

Mathematically, the conditions described above are translated into

$$w = u\frac{\partial z_b}{\partial x} + v\frac{\partial z_b}{\partial y} \quad z = z_b \tag{A.14}$$

$$w = \frac{\partial z_s}{\partial t} + u\frac{\partial z_s}{\partial x} + v\frac{\partial z_s}{\partial y} \quad z = z_s \tag{A.15}$$

$$\nu_v \left(\frac{\partial u}{\partial z}\right)_{z=z_b} = \frac{\tau_{b,x}}{\rho_0} \tag{A.16}$$

$$\nu_v \left(\frac{\partial v}{\partial z}\right)_{z=z_b} = \frac{\tau_{b,y}}{\rho_0} \tag{A.17}$$

$$\overrightarrow{\tau_b} = \rho|\overrightarrow{u_*}|\overrightarrow{u_*} = \frac{\rho_0\kappa^2|\overrightarrow{u_b}|}{\ln\left(1+\frac{\Delta z_b}{z_0}\right)}\overrightarrow{u_b} \tag{A.18}$$

$$\nu_v \left(\frac{\partial u}{\partial z}\right)_{z=z_s} = \frac{|\overrightarrow{\tau_w}|}{\rho_0}\sin\phi \tag{A.19}$$

$$\nu_v \left(\frac{\partial v}{\partial z}\right)_{z=z_s} = \frac{|\overrightarrow{\tau_w}|}{\rho_0}\cos\phi \tag{A.20}$$

$$\overrightarrow{\tau_w} = \rho_{air} c_d |\overrightarrow{U_{10}}|\overrightarrow{U_{10}} \tag{A.21}$$

where,

| | |
|---|---|
| $z_b$ | the bed level, |
| $z_0$ | the water level, |
| $\tau_{b,x}, \tau_{b,y}, \tau_b$ | the bed shear stress in $x$ and $y$ direction, and the sum of the two vectors, respectively, |
| $\tau_w$ | the surface shear stress in the forcing direction (here due to the wind), |
| $\rho_{air}$ | the density of air, |
| $c_d$ | the drag coefficient due to the movement of air, |
| $\phi$ | the angle between the $y$ direction and the direction of the forcing, |
| $u_b$ | velocity at $z_0$, |
| $u_*$ | shear velocity, |
| $U_{10}$ | the wind velocity at 10 m above the water surface. |

Except for the water-surface boundary condition, more open boundary conditions are necessary for solving the flow in a river reach. These boundaries are usually artificial, but necessary for restricting the domain in a part of a reach. The number of this type of open boundary conditions needed for solving a problem can be different for a numerical simulation and the mathematical equation being modelled. For the mathematical system, it depends on the propagation of the solution, whereas in numerical modelling it depends

on the stencil being applied. As a result, the mathematical boundary conditions could vary in time, but for the numerical model this is not necessary.

They are distinguished into gradient-type or Neumann boundary conditions, where the gradient of the solution along the boundary is imposed, fixed or Dirichlet boundary conditions, which provide the exact solution at the boundary, and combinations of the two (Robin boundary conditions).

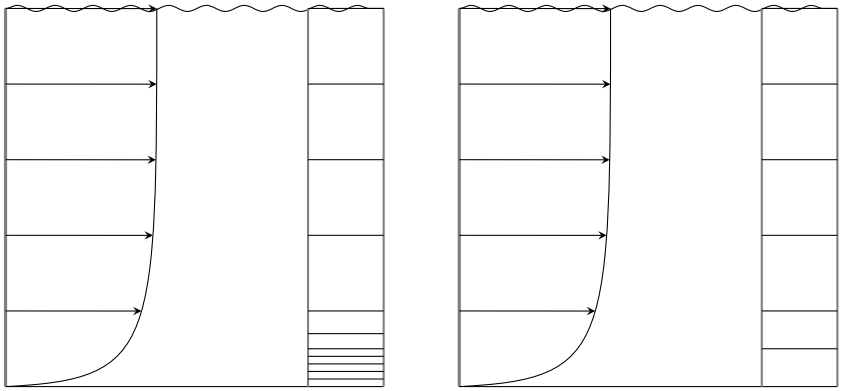

Figure A.3: Schematization of the grid structure depending on the boundary condition. On the left the boundary layer is resolved and on the right it is modelled.

### A.1.3 Depth averaging the 3D shallow-water equations (SWE)

In the 2DH SWE, Equation A.11, Equation A.12, and Equation A.13 are depth averaged. Firstly, the depth averaged velocities are defined as,

$$U_i = \int_{z_b}^{z_s} u_i \mathrm{d}z \quad i = 1, 2 \tag{A.22}$$

With the help of the kinematic boundary conditions (Equation A.15), with the definition of the depth-averaged velocity (Equation A.22) and after applying the Leibniz rule the depth-averaged SWE are computed. The main implication of this procedure is that with the definition of the depth-averaged velocity, we are not able to compute the integrals of the gradients of the quadratic velocities $(uu, uv, uw, vv, vw)$. These terms contain the information of dispersion of momentum due to velocity fluctuations in the vertical. Essentially, they contain the information regarding the redistribution of momentum in the case of curved flow due to secondary flow. Attention has to be paid also for the bed shear stress that depends on the near-bed velocity gradient but is usually computed from the depth-averaged velocity. As a result, decomposing the velocities (similarly with the

'Reynolds decomposition'), we get,

$$u_i = U_i + u_i^* \quad i = 1, 2 \tag{A.23}$$

with $u_i^*$ the deviation of the real velocity from its depth-averaged value in the vertical. The 2D SWE then read ($U_1 \to U$, $U_2 \to V$, $u_i^* = u_i - U_i$),

$$\frac{\partial z_s}{\partial t} + \frac{\partial hU}{\partial x} + \frac{\partial hV}{\partial y} = 0 \tag{A.24}$$

$$\frac{\partial U}{\partial t} + U\frac{\partial U}{\partial x} + V\frac{\partial U}{\partial x} + \boxed{\frac{\partial \frac{1}{h}\int_{z_b}^{z_s}(u-U)^2\,\mathrm{d}z}{\partial x}} + \boxed{\frac{\partial \frac{1}{h}\int_{z_b}^{z_s}(u-U)(v-V)\,\mathrm{d}z}{\partial y}} = \nu_h\left(\frac{\partial^2 U}{\partial x^2} + \frac{\partial^2 U}{\partial y^2}\right) - g\frac{\partial z_s}{\partial x} - \frac{\tau_{b,x}}{\rho_0 h} + fV + \frac{\tau_{w,x}}{\rho h} - \frac{1}{\rho_0}\frac{\partial p_{atm}}{\partial x} \tag{A.25}$$

$$\frac{\partial V}{\partial t} + U\frac{\partial V}{\partial x} + V\frac{\partial V}{\partial y} + \boxed{\frac{\partial \frac{1}{h}\int_{z_b}^{z_s}(v-V)^2\,\mathrm{d}z}{\partial x}} + \boxed{\frac{\partial \frac{1}{h}\int_{z_b}^{z_s}(u-U)(v-V)\,\mathrm{d}z}{\partial y}} = \nu_h\left(\frac{\partial^2 V}{\partial x^2} + \frac{\partial^2 V}{\partial y^2}\right) - g\frac{\partial z_s}{\partial y} - \frac{\tau_{b,y}}{\rho_0 h} - fU + \frac{\tau_{w,y}}{\rho h} - \frac{1}{\rho_0}\frac{\partial p_{atm}}{\partial y} \tag{A.26}$$

with $h$ the water depth ($h = z_s - z_b$). The extra dispersion terms (terms inside boxes) either are neglected or have to be modelled, because there is no information on the vertical velocity profile. Neglecting them or assuming that they are incorporated inside the turbulent viscosity coefficient is reasonable if we assume small variations in the vertical profiles in space and time. This is not the case though for curved open-channel flow. These terms have to be modelled by a secondary-flow closure submodel.

### A.1.4 Secondary flow

In the case of river bends the dispersion fluxes are crucial for the redistribution of momentum along the bend due to the secondary flow. Secondary flow is defined as the deviation from a standard vertical distribution of the flow velocities. In 2D modelling the vertical velocity profile is not solved, and as a result a closure relationship has to be defined in order to simulate the velocity redistribution due to flow curvature.

In the context of river bends, it is important to express the velocities in the directions of

the depth-averaged velocity, and in the direction transverse to it. In this way, the velocities are split into the main-flow component and the secondary-flow component. In the case of fully developed flow, the streamlines follow the boundaries of the river, assuming constant curvature and channel width. As a result, in that region, transforming the hydrodynamic equations into a curvilinear coordinate system which follows the channel boundaries, allows the expression of the conservation equations for mass and momentum in relation with the mean and the secondary-flow components.

Various proposals exist in literature for the calculation of the secondary flow in river bends. Generally, a constant curvature bend with uniform width is assumed. A common line of work for solving the closure problem using the perturbation theory is:

1. The three-dimensional system of equations that describe the flow field is transformed from a Cartesian to a polar coordinate system following the streamwise direction (curvilinear or cylindrical).

2. The momentum equations in the downstream and the cross-flow direction are simplified assuming fully developed flow (neglecting spatial and time variations, solving the conservation equations only in the centerline) and as a result the streaklines coincide with the streamlines. A definition profile for the vertical eddy viscosity is also necessary.

3. An order-of-magnitude analysis is performed and a perturbation parameter is defined ($h/R$ for linear closure submodels).

4. Either an analytical solution is found for the secondary flow, or the system of the horizontal momentum balance equations is solved numerically with the help of an asymptotic expansion (Olesen, 1987).

5. The calculated secondary-flow profile corresponds to the fully developed conditions at the centerline. As a result a relaxation model has to be applied for calculating the secondary flow in streamwise direction and a distribution function along the width.

The major distinction of the secondary-flow models is related with their validity. All are valid within the mild-curvature limit, whereas there is recently more interest in developing submodels for bends with sharper curvatures. This is an immediate result of the order-of-magnitude analysis and the neglected terms. The models that are only valid in the mild-curvature limit, also called linear closure submodels, neglect the non-linear feedback between the helical and the main flow, and eventually overpredict the secondary flow velocities. According to Blanckaert (2009) there is a limit at which the secondary flow does not further increase with decreasing the radius of curvature of a channel bend (saturation of the secondary flow.) This can be captured only with non-linear secondary-flow submodels.

## A.2 Sediment transport

Sediment transport forms the link between the flow and the bed level changes. In the context of this thesis, it is defined as the sediment that is in motion in an alluvial river. The accuracy of the morphological predictions strongly depends on the methods used for estimating the displacement, magnitude, and transport of sediment.

The classification of sediment can be done based on grain size and chemical synthesis. For the morphologist, an important distinction is based on the existence or not of chemical processes between the individual particles. In this way cohesive and non-cohesive sediment are defined. Both can be directly involved in morphological changes, but due to their different behaviour only the first will be considered in the remainder of this thesis. Sediment transport is classified based on its origin, properties, and transport mechanism (Figure A.4). Based on origin, washload is defined as the material with smaller grain size than the bed material (Jansen et al., 1979). Effectively, washload is considered not to contribute to morphological changes. Despite the above, a quantitative distinction between washload and bed-material load is important. This can be justified in several ways. One of them is for calibration of the applied sediment transport formula with field measurements (De Vries, 1993). Another important reason is that, according to the definition of washload that was given above, washload can often become bed-material load or vice versa. The division between bed load and suspended load however, is influenced by the grain size, the flow, and the topographic conditions. Physically, a grain which is in suspension is assumed to be travelling with the flow velocity, whereas a grain which is transported as bed load may move only occasionally, especially near the limit of the mobility of sediment as defined by Shields (1936). Moreover, the same grain particle could belong to bed load or suspended load, based on its location at a given time. This makes a distinction vague and different definitions exist as already discussed in Chapter 1. In order to conceptualize the transport modes mathematically, a reference height $a$, above the bed is defined, which divides suspended and bed load sediment.

The distinction between bed load and suspended load allows a separate treatment of the processes. It is common to assume that the bed load instantaneously adapts to the local flow conditions. The transported amount therein will be based on the flow capacity, as given by a sediment transport model. This is not the case for the suspended sediment. Adaptation length and time scales are necessary in order to simulate its behaviour. This is a result of the vertical length of the suspended sediment region.

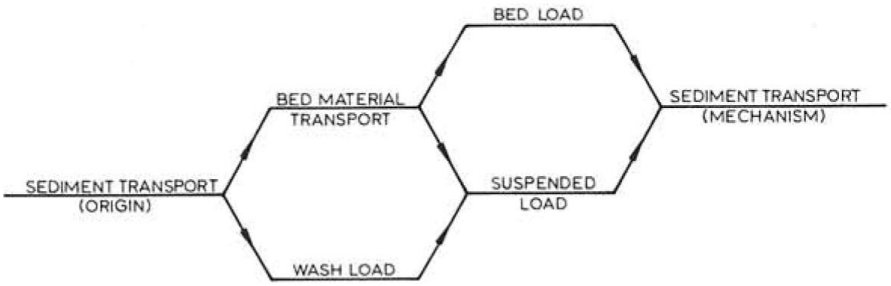


Figure A.4: Sediment classification based on origin and transport mechanism (Jansen, Van Bendegom, Van den Berg, De Vries, & Zanen, 1979).

### A.2.1 Sediment transport formulas

Sediment transport formulas act as predictors of the sediment transport capacity based on local flow quantities. They provide the magnitude of sediment in transport and ignore adaptation lengths and time scales. A non-cohesive sediment grain is in motion if the total force and torque due to its weight, forces due to the flow, and due to adjacent grains are zero. When the total force or the torque around a center of rotation just becomes non-zero the sediment is moving. This is called the incipient sediment motion. Some formulas assume that there is a threshold below which no sediment transport is possible, and are called deterministic or MPM-type (Van Rijn, 1984a, 1984b, 1984c; Meyer-Peter & Müller, 1948). Others do not assume a threshold value for the incipient motion, but rather consider it a stochastic phenomenon due to the stochastic nature of the turbulent eddies in addition to the unknown individual grain properties. They are called stochastic.

According to the sediment mode taken into account, sediment transport formulas can be divided into three categories:

- formulas predicting only bed load sediment transport,
- formulas predicting both bed load and suspended load sediment transport, explicitly separating them, and
- formulas predicting the total load consisting of both bed load and suspended load sediment transport.

In straight channels, the retarded adaption of suspended load can be neglected if the adaptation length and time scales are short enough. A criterion as defined in Mosselman (2005) for numerical modelling is that if the adaptation length scale is smaller than $2-3$ times the computational cell, the retarded adaption of suspended load can be ignored. In curved channels although, the mode of suspended sediment cannot be ignored due to the

fundamentally different mechanism that determines its direction due to the differences in the resulting wavenumber and damping of the solution.

It is common to straightforwardly assume that the bed load sediment transport magnitude is equal to the one given by the sediment transport formula applied. But in order to model adaptation length and time scales for suspended sediment, we have to apply the mass conservation principle in the concentration of sediment inside the water column from a reference height $a$ to the water surface. Hence, the reference height splits the water column into two layers, the suspended-sediment layer, and the bed-load layer. The role of the sediment transport formula in which suspended load is defined, is to assist deriving a relation for the sediment concentration at the reference height plane (near-bed boundary condition).

A general form of sediment transport formulas can be

$$s = mu^n \tag{A.27}$$

where $s$ is the sediment transport rate per unit width and $a, b$ are coefficients dependent on the formula applied.

### A.2.2 Bed-load transport direction

Adaptation lengths and time scales for bed load transport are ignored. With this hypothesis, modelling bed load transport direction does not require the same, computationally intensive, procedure as modelling suspended load. The magnitude of bed load is computed equal to the one provided by the sediment transport model applied. Diffusive transport is also ignored, and the driving mechanisms that determine the direction are the bed shear stress due to the water flow and the gravity pull along a sloping bed (bed slope effect). In curved open channels, the bed shear stress direction differs from the depth-averaged flow velocity, due to the secondary flow. The net non-zero transverse stress component leads to the non-zero transverse bed slope, which leads to the "push" of the higher velocities in the outer-bend region and the convection of fast flowing water towards the outer bank. Finally, this process further increases the transverse bed slope and the gravity pull along the transverse bed slope becomes more important. The bed slope effect for an initially non-moving or rolling grain is translated in a gravitational force component parallel to the bed. For a saltating grain, the bed slope effect arises from the influence of its position after approaching the bed with an impact angle. For an extensive analysis on the subject reference is made to Olesen (1987). He proposed the general solution for the angle between

the bed load sediment transport vector and the depth-averaged flow vector to be given by,

$$\tan a = A\frac{h}{R} - \frac{1}{f(\theta)}\frac{\partial z_b}{\partial n} \tag{A.28}$$

where

| | |
|---|---|
| $a$ | the angle between the bed load transport vector and the depth-averaged flow vector, |
| $f(\theta)$ | factor for bed slope effect (as a function of Shields parameter), |
| $R$ | curvature of the streamline, |
| $\frac{\partial z_b}{\partial n}$ | transverse bed slope, and |
| $A$ | coefficient accounting for the effect of spiral flow on the direction of bed shear stress |
| $h$ | flow depth. |

### A.2.3 Suspended load transport direction

The mass balance of sediment concentration inside the water column (neglecting its influence on the water density) reads

$$\frac{\partial c}{\partial t} + \frac{\partial uc}{\partial x} + \frac{\partial vc}{\partial y} + \frac{\partial (w - w_s)c}{\partial z} = \frac{\partial}{\partial x}\left[\epsilon_{sx}\frac{\partial c}{\partial x}\right] + \frac{\partial}{\partial y}\left[\epsilon_{sy}\frac{\partial c}{\partial y}\right] + \frac{\partial}{\partial z}\left[\epsilon_{sz}\frac{\partial c}{\partial z}\right] \tag{A.29}$$

with,

| | |
|---|---|
| $c$ | the suspended sediment concentration, |
| $w_s$ | the fall velocity of sediment, and |
| $\epsilon_{sx}, \epsilon_{sy}, \epsilon_{sz}$ | the diffusion coefficients in $x, y$ and $z$ directions, respectively. |

In order to solve Equation A.29, the boundary conditions at the water surface and the bed have to be defined. At the water surface the zero flux of sediment concentration is applied (no exchange of sediment between the water and the air) as shown in Equation A.30.

$$\left|\epsilon_{sz}\frac{\partial c}{\partial z} + cw_s\right|_{z=z_s} = 0 \tag{A.30}$$

Near the bed, two possibilities exist. The first possibility is that the concentration at the reference level $\alpha$ is equal to the concentration computed by the sediment transport formula

(Equation A.31). The second possibility is that the gradient of sediment concentration is zero (Equation A.32).

$$|c|_{z=z_b+\alpha} = c_b \tag{A.31}$$

$$\left| -\epsilon_{sz} \left( \frac{\partial c}{\partial z} \right) \right|_{z=z_b+\alpha} = w_s c_b \tag{A.32}$$

with $c_b$ the near bed reference concentration as calculated with the help of a sediment transport model.

Depth-averaging the convection-diffusion equation for suspended sediment is not straightforward. The main complication is a result of the unknown vertical sediment concentration profile, and the near-bed boundary condition. Either a semi-empirical condition is needed, or an asymptotic approximation of the concentration field according to the 2DV or 3D convection-diffusion equation, originally proposed by Galappatti (1983). Moreover, during the averaging procedure, the dispersion of sediment concentration due to variations in the vertical of the velocity and the concentration profile are ignored if no special attention is given. This is analogous to the dispersion of momentum after depth averaging the 3D SWE.

In the case of river bends, this has a prominent effect on the predicted morphology when suspended sediment load is included. It can intuitively be understood, as shown in Figure A.5, that deviations in the vertical secondary-flow profile, along with the non-uniform sediment concentration, will lead to a net non-zero transverse transport component.

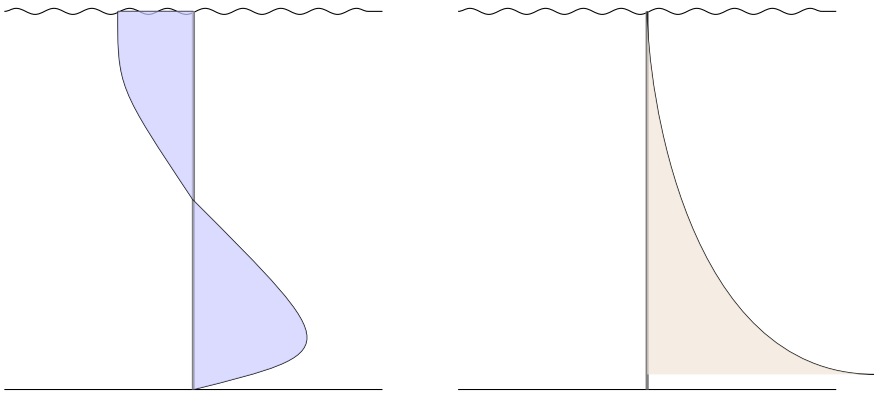

Figure A.5: Schematization of the secondary flow profile (left figure) and the suspended sediment concentration profile (right figure).

## A.3 Bed level change

Bed level variations are an immediate result of the water flow. This is an interrelated condition, as changes in the geometry of the problem affect the hydrodynamic processes. The quasi-steady flow principle allows the decoupling of the hydrodynamic computations from the bed level changes. Based on mathematical analysis of the one-dimensional, simplified shallow-water equations, only with bed load transport (De Vries, 1959, 1965), it is proven that the assumption is allowed for $Fr < 0.8$. More specifically, the relative celerity of disturbances in the flow is much larger than the one for disturbances in the bed surface. The relative celerity it is defined as

$$\phi = c/u \tag{A.33}$$

with $c$ the propagating celerity of the characteristics, which reads,

$$c = \frac{\mathrm{d}x}{\mathrm{d}t} \tag{A.34}$$

Figure A.6 shows the relation between relative celerities and the Froude number, $Fr$, for different values of a nondimentional transport parameter. The Froude number is defined as

$$Fr = \frac{u}{\sqrt{gh}} \tag{A.35}$$

The transport parameter is defined as the ratio of the celerity of bed disturbances to flow velocity for $Fr \ll 1$. For a sediment transport formula of the form of Equation A.27, the transport parameter can be written as

$$\psi = b\frac{s}{q} \tag{A.36}$$

with $q$ the flow discharge per unit width.

### A.3.1 The Exner equation

Ignoring sediment sorting processes, bed level variations can be computed with the Exner equation. The equation is derived from the mass balance of sediment. Conceptually, it is translated as that the bed level changes in time are a result of the space variations of the

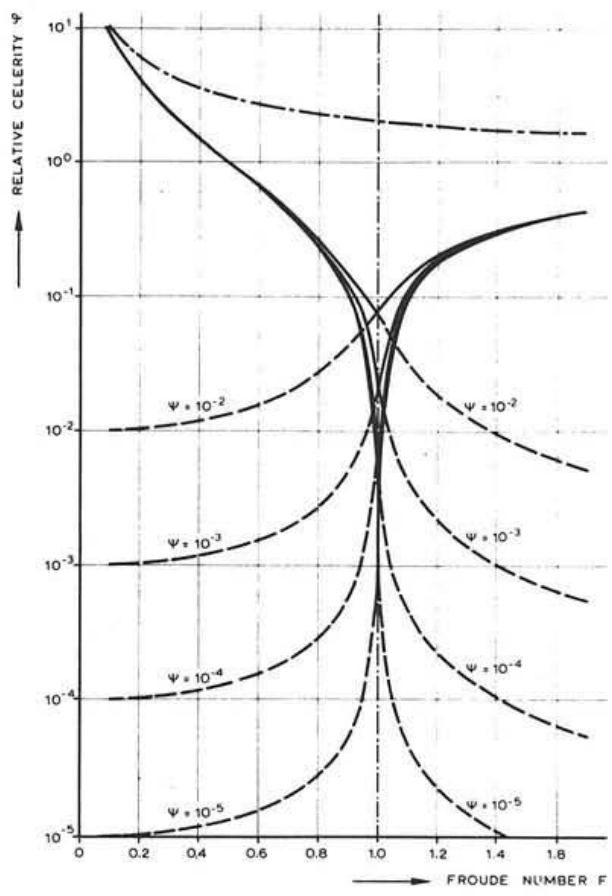


| SYMBOL | REGARDS | SIGN. | |
|---|---|---|---|
| | | F<1 | F>1 |
| —·— | WATER LEVEL | + | + |
| ——— | WATER LEVEL | − | + |
| – – – | BED LEVEL | + | − |

Figure A.6: Quasi-steady bed assumption; relative celerity of disturbances in relation with the Froude number (Jansen, Van Bendegom, Van den Berg, De Vries, & Zanen, 1979).

sediment transport magnitude, because the excess or lack of sediment out of the control volume has to have settled in the bed. In other words,

$$\frac{\partial z_b}{\partial t} + \frac{\partial hC}{\partial t} + \frac{\partial s_b^x}{\partial x} + \frac{\partial s_b^y}{\partial y} + E - D = 0 \tag{A.37}$$

where

$s_b$ bulk bed load sediment transport per unit width

$E$ erosion rate of sediment per unit width; sink from the bed to the water column as suspended sediment,

$D$ deposition rate of sediment per unit width; source to the bed from the water column, due to suspended sediment transport.

The second term of Equation A.37 ($\frac{\partial hC}{\partial t}$) is not easily and accurately computed when the morphological time scale is assumed to be much larger than the time scale on which the depth-averaged concentration changes. As a result, it can either be explicitly computed assuming that the gradient on the large time scale is the same as the gradient on the small one, or it is ignored (small influence on the solution). Instead of computing the bed level changes with the erosion and deposition rates of suspended sediment, we can also apply,

$$\frac{\partial z_b}{\partial t} + \frac{\partial hC}{\partial t} + \frac{\partial s_b^x}{\partial x} + \frac{\partial s_b^y}{\partial y} + \frac{\partial s_{sus}^x}{\partial x} + \frac{\partial s_{sus}^y}{\partial y} = 0 \tag{A.38}$$

where $s_{sus}$ denotes the bulk suspended sediment transport per unit width.

# Appendix B

# Simulation settings and results

## B.1 Numerical experiments

### B.1.1 Hypothetical bend experiments

The domain consists of two straight sections with one circular bend of 180 degrees. The set-up of the simulations in shown in Table B.1 ($W$ is the width of the cross-section, $R$ is the radius of curvature at the centreline, $Q$ is the discharge, $i$ the bed slope, $h$ the equilibrium water depth, $C$ the Chézy smoothness coefficient, and $d_{50}$ the characteristic grain diameter.) The 3D model consists of 30 equidistant layers.

Table B.1: Data for the hypothetical bend experiments.

| | Hypothetical bend |
|---|---|
| $Q$ | $1020\,\mathrm{m^3\,s^{-1}}$ |
| $h$ | $10\,\mathrm{m}$ |
| $i$ | $5 \times 10^{-5}$ |
| $C$ | $50\,\mathrm{m^{0.5}\,s^{-1}}$ |
| $d_{50}$ | $200\,\mu\mathrm{m}$ |
| $W$ | $100\,\mathrm{m}$ |
| $R$ | $1000, 2000, 4000\,\mathrm{m}$ |

The semi-empirical secondary-flow profiles using the modified version of Delft3D are compared with the ones from the 3D simulations (Figure B.2, Figure B.4, and Figure B.6). As it was expected, the initial small error in the spiral flow intensity results in a larger error in equilibrium conditions in the outer-bend region, and a smaller error in the inner-bend region. After that, the water depths are normalized with the water depth at the entrance of the bends, and the equilibrium solutions are plotted (Figure B.3a, Figure B.5a, and Figure B.7a). The wave length is shown to be much larger for the case with suspended

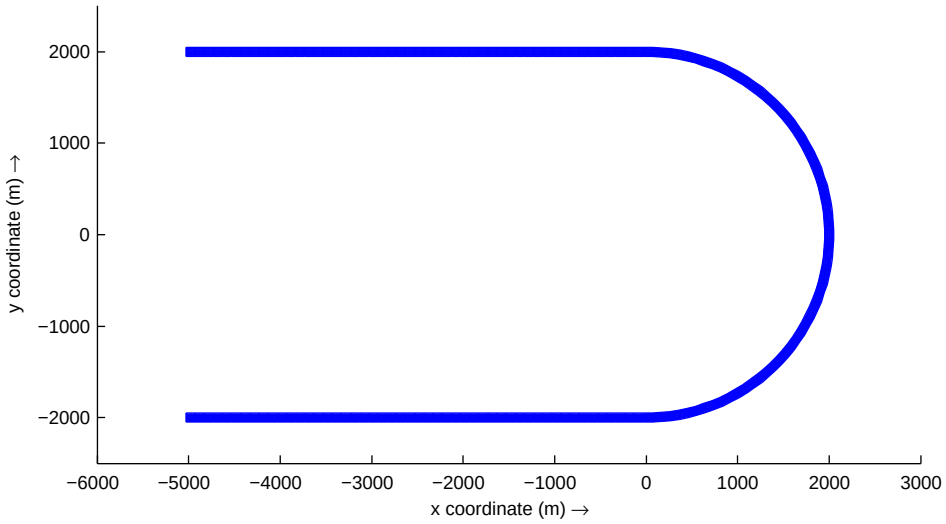


Figure B.1: Domain of hypothetical bend experiments for $R = 2000\,\mathrm{m}$.

sediment transport than the case with bed load only. Although the different sediment transport formula applied has an influence, the most important reason is considered to be the different behaviour of the solution because of the presence of suspended sediment transport. The modified version of Delft3D (2DH total-load modified Delft3D) has almost the same solution with the 3D simulation (3D total-load) except for the case where $R = 1000\,\mathrm{m}$.

Finally the normalized water depth near the exits of the bends, where they more closely approach an axi-symmetric solution, are plotted and compared (Figure B.3b, Figure B.5b, and Figure B.7b). It can be noticed:

- The transverse bed slope in the 3D simulation with suspended sediment transport (3D total load) is considerably larger than the case where only bed load is modelled.
- In the default version of Delft3D, the transverse bed slope decreases when suspended sediment transport is included with a depth-averaged simulation (2DH default Delft3D). As the analysis of the axi-symmetric solution has shown (Chapter 2), this is caused by the diffusive transport of suspended sediment.
- The modified version of Delft3D performs accurately with exception of the outer-bank region where the accuracy decreases with decreasing radius of the bend.

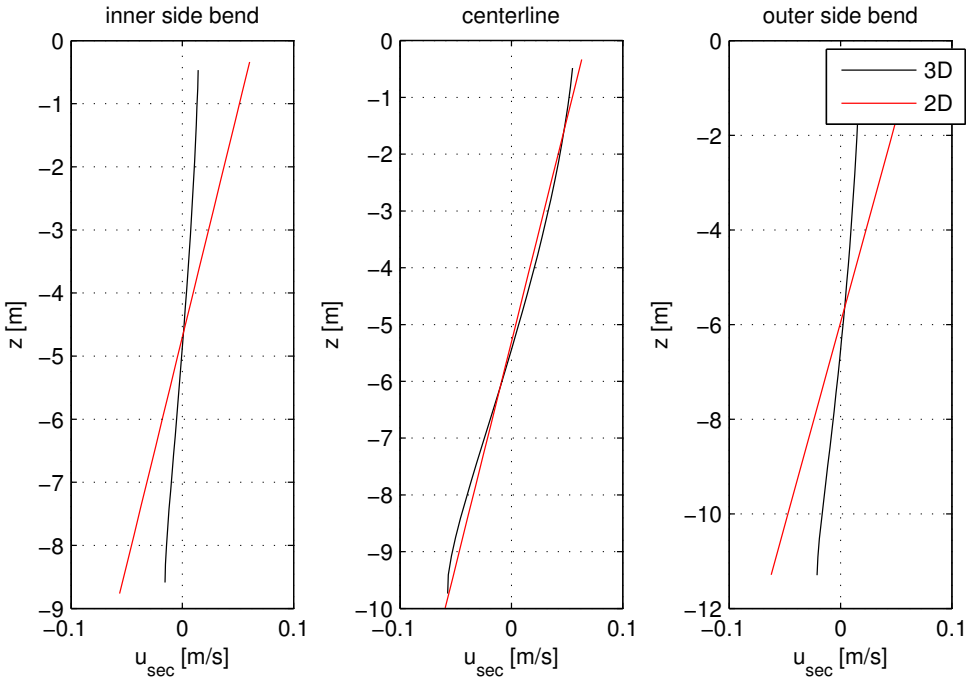


(a) $t = 50\,\mathrm{d}$.

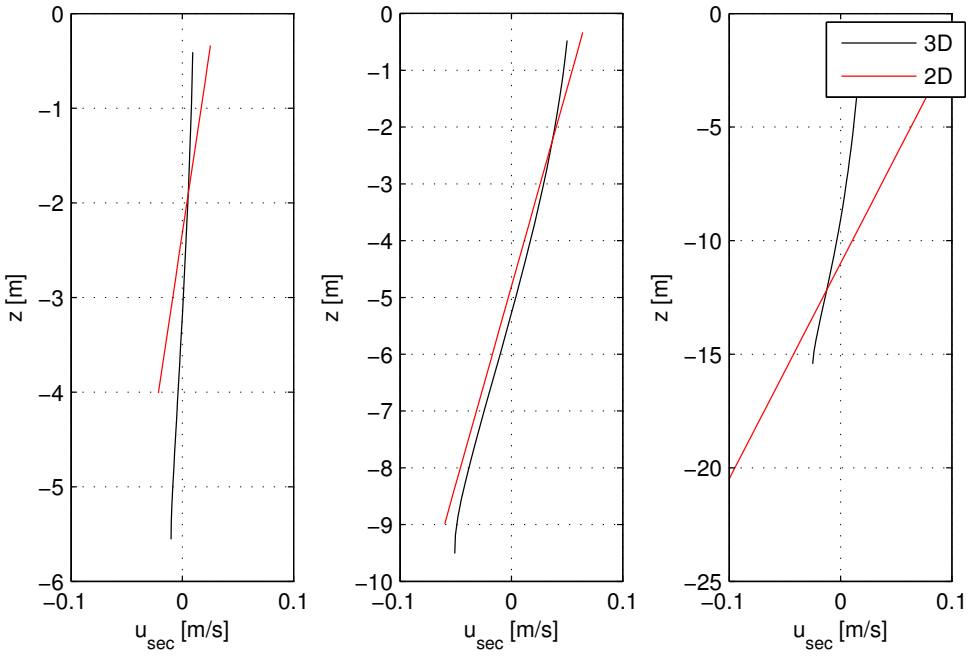


(b) $t = 30\,\mathrm{yr}$.

Figure B.2: Secondary flow profiles near the exit of the bend $R = 1000\,\mathrm{m}$.

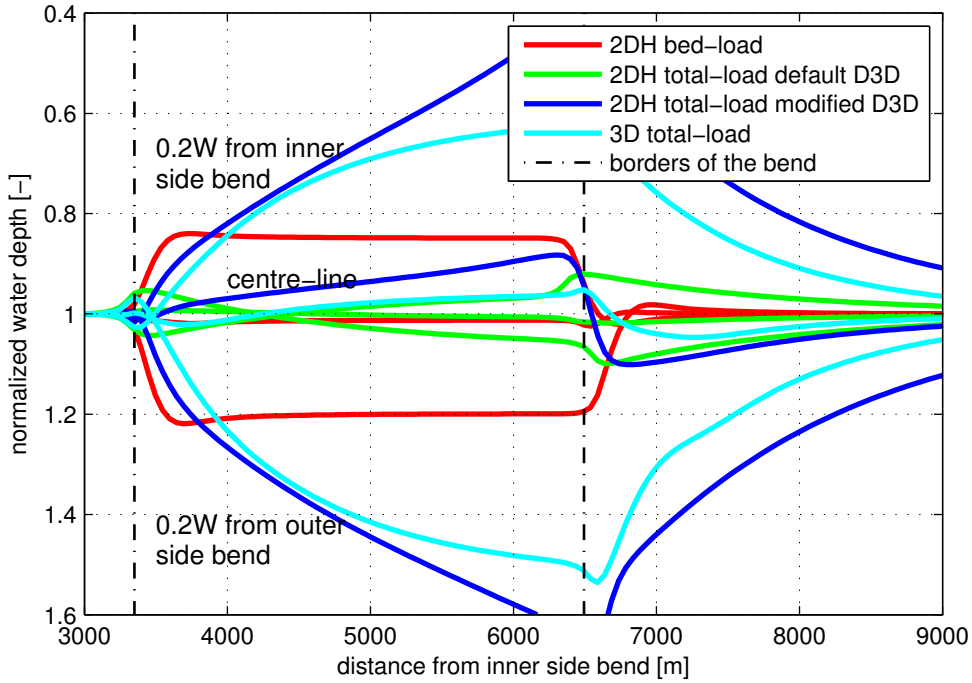


(a) Streamwise profiles.

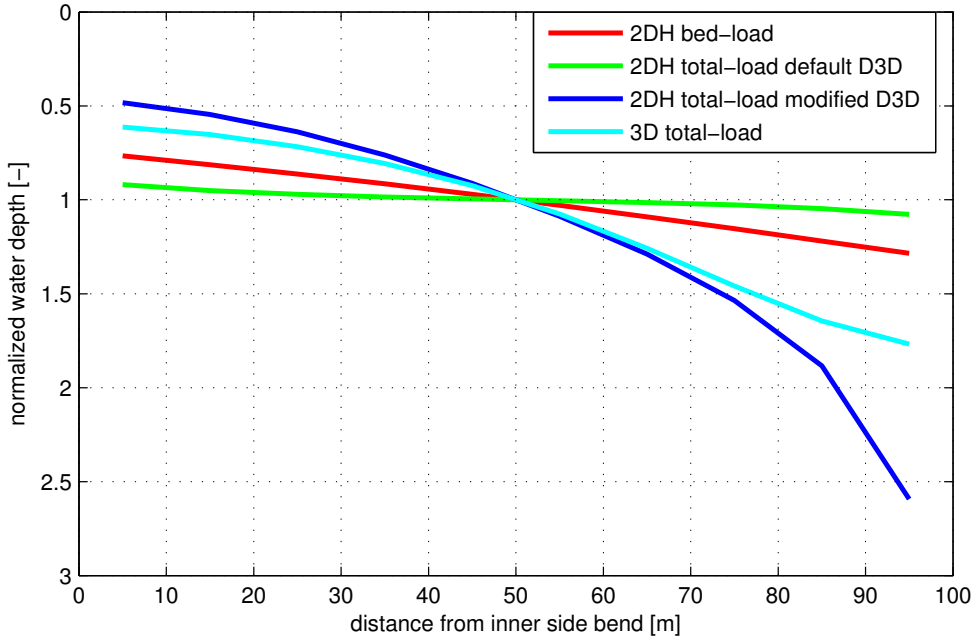


(b) Cross-section near the exit of the bend.

Figure B.3: Equilibrium solution $R = 1000\,\mathrm{m}$.

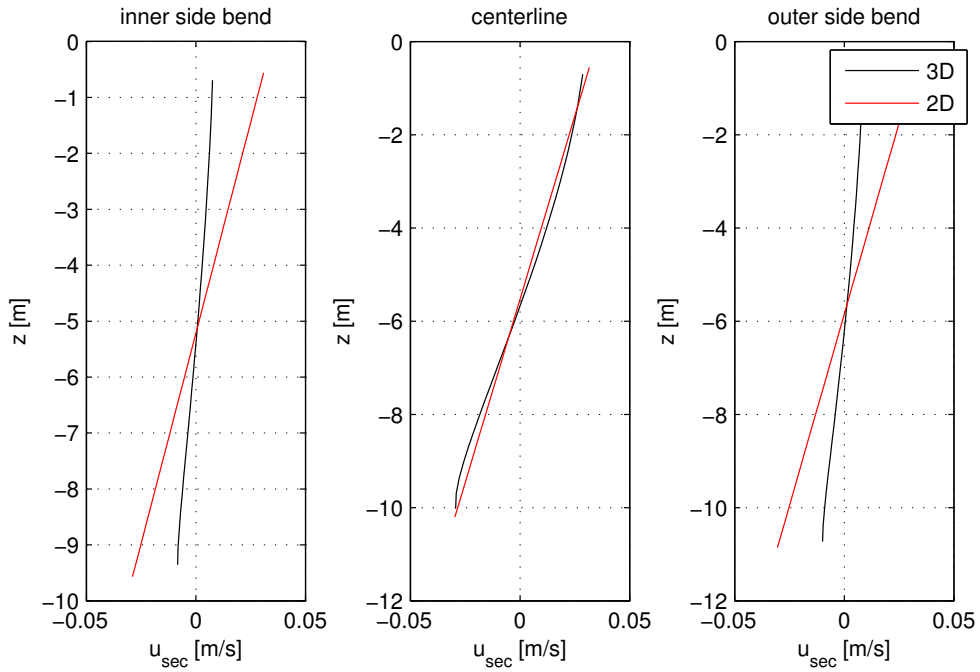


(a) $t = 50\,\mathrm{d}$.

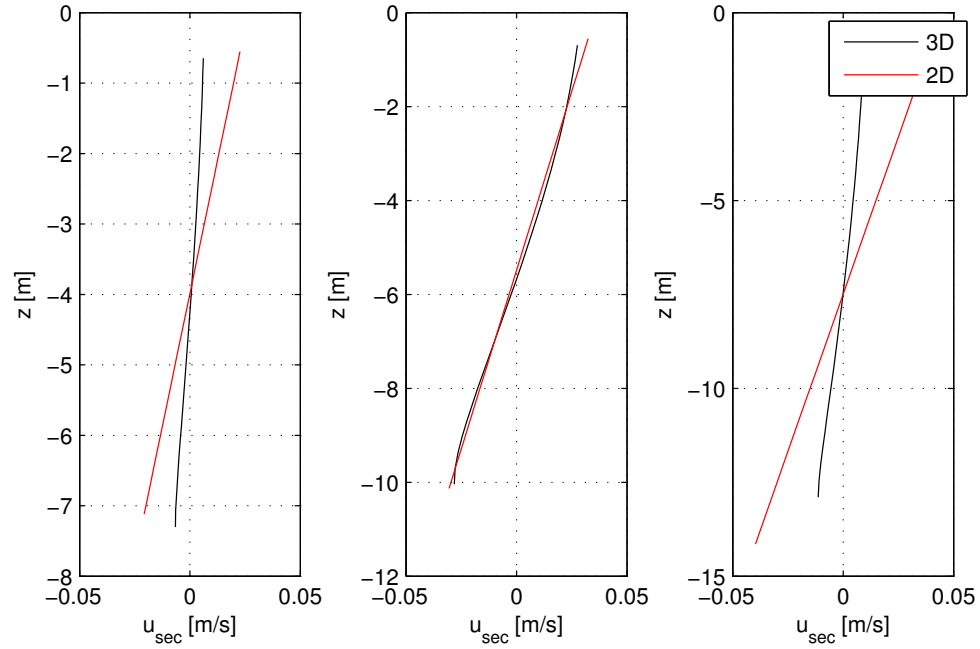


(b) $t = 30\,\mathrm{yr}$.

Figure B.4: Secondary flow profiles near the exit of the bend $R = 2000\,\mathrm{m}$.

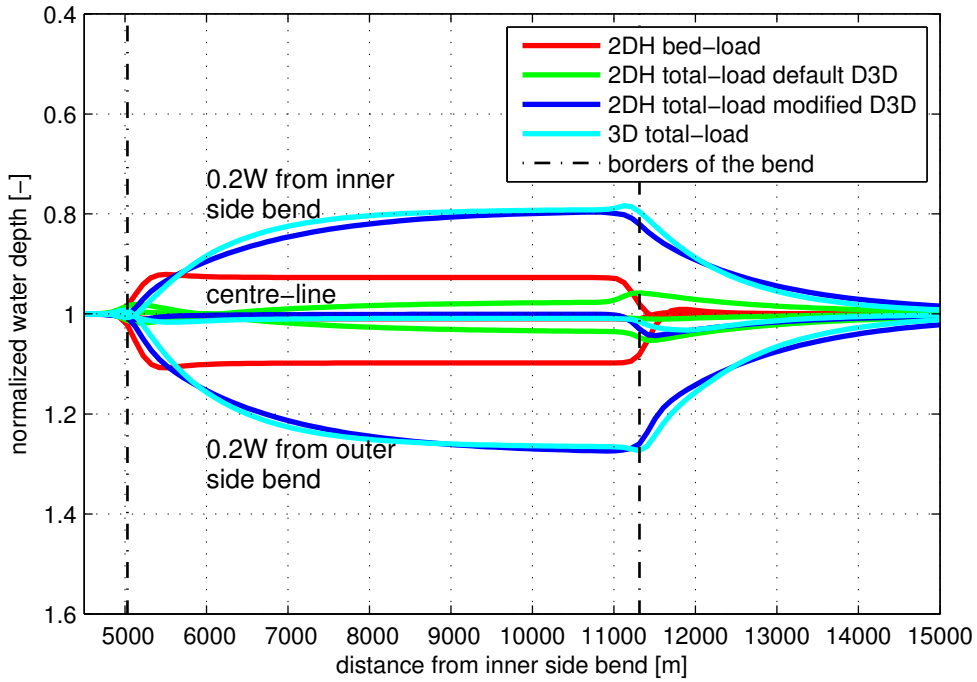


(a) Streamwise profiles.

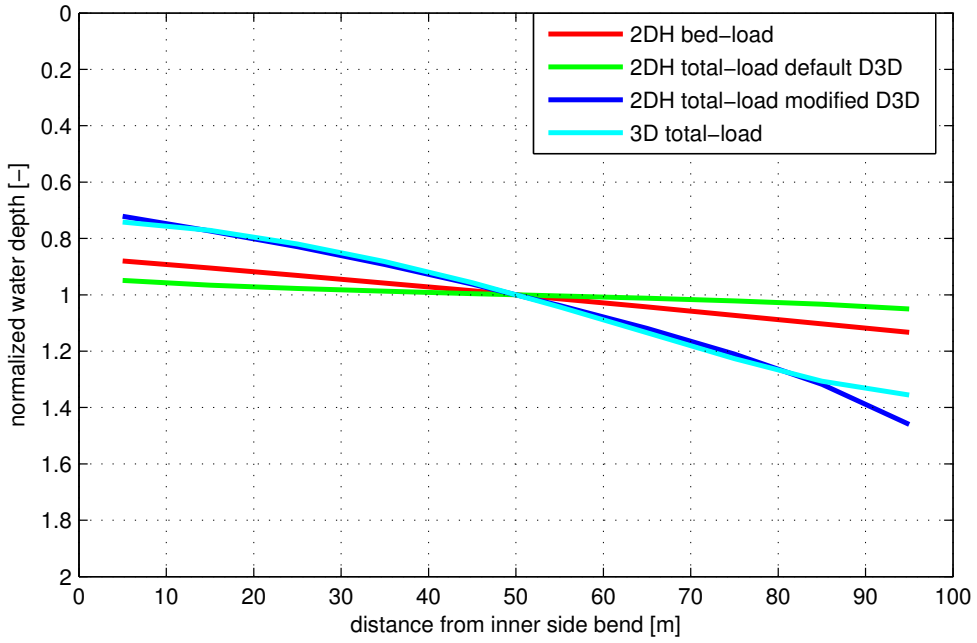


(b) Cross-section near the exit of the bend.

Figure B.5: Equilibrium solution $R = 2000\,\mathrm{m}$.

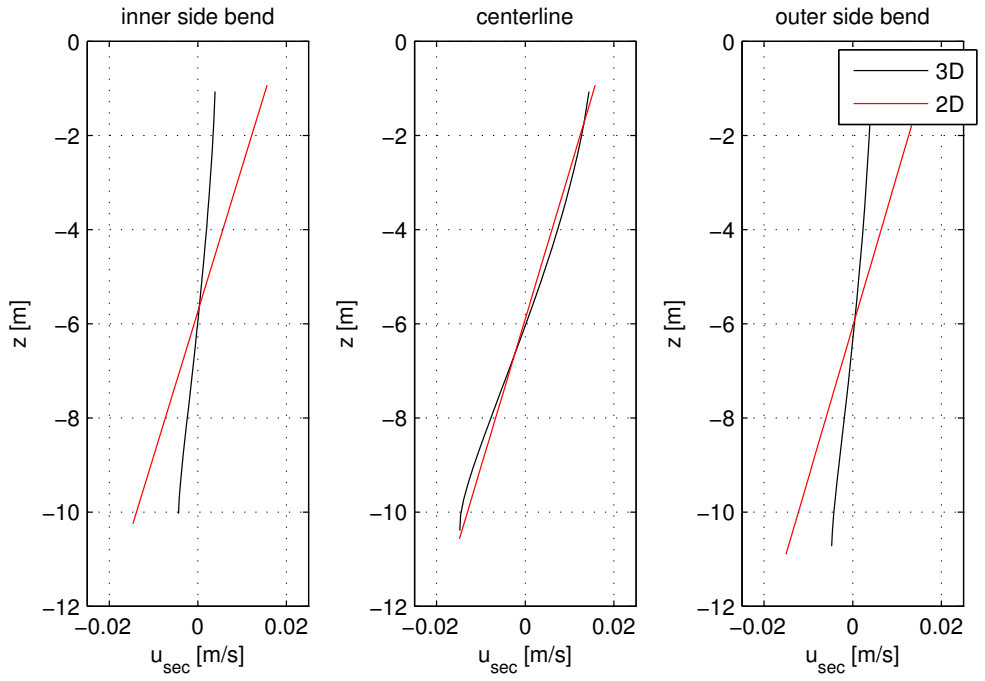


(a) $t = 50\,\mathrm{d}$.

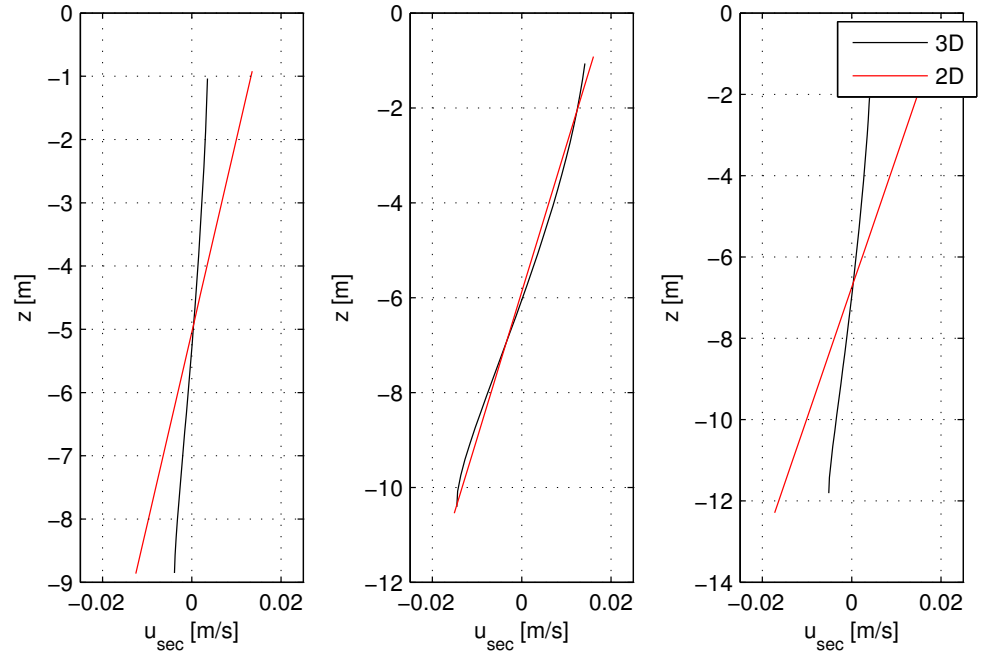


(b) $t = 30\,\mathrm{yr}$.

Figure B.6: Secondary flow profiles near the exit of the bend $R = 4000\,\mathrm{m}$.

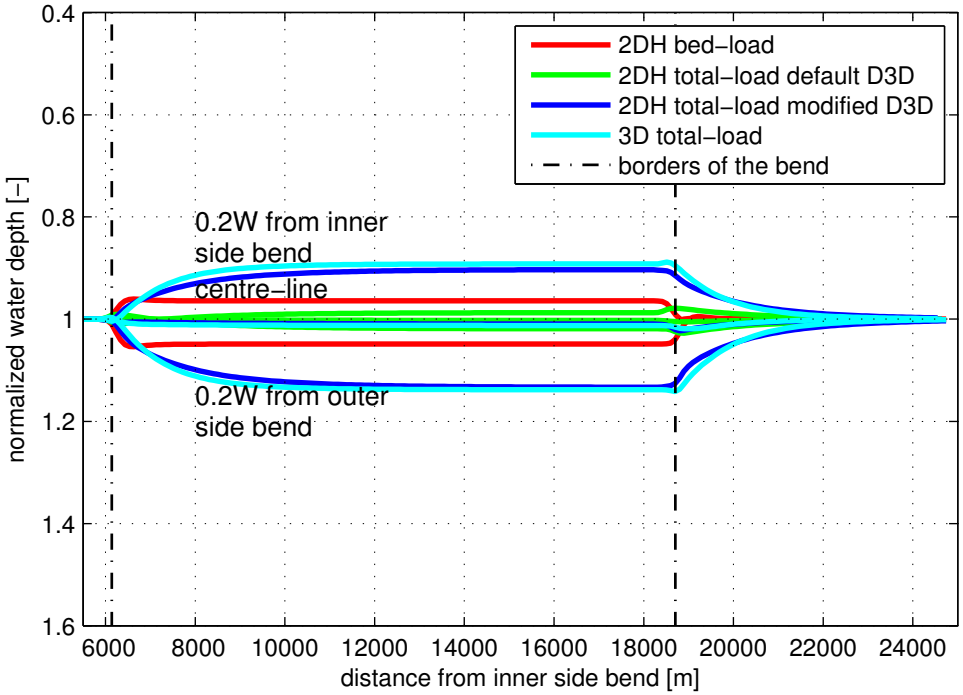


(a) Streamwise profiles.

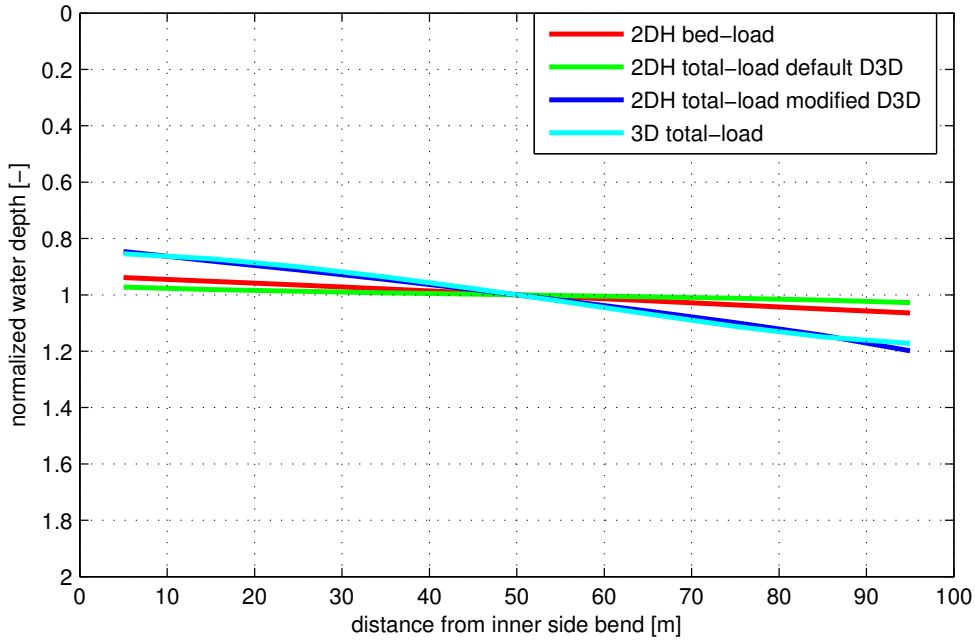


(b) Cross-section near the exit of the bend.

Figure B.7: Equilibrium solution $R = 4000\,\mathrm{m}$.

### B.1.2 Flume experiments

Datasets of curved-flume experiments including suspended sediment transport were available thanks to Talmon (1992). While the suspended sediment load was more or less of the same order of magnitude as the bed load, and as a result the modifications to Delft3D are not expected to be crucial, it is still interesting to investigate the performance of the model compared to real data. The results from 3D simulations do not necessarily represent the natural behaviour of a system. The 6 different scenarios were carefully designed (the first 4 will be simulated; run 1-4). The stationary bed topographies measured are compared with the model results. For run 2 and run 4 an axi-symmetric region is present, while for run 1 and run 3 the damping is smaller and two point-bars develop. For more details on the experiments reference is made to Talmon (1992). The radius of the bend at the centerline of the flume is $R = 4.1\,\mathrm{m}$ and the width is $W = 0.5\,\mathrm{m}$. The settings of the experiments are shown in Table B.2. The first two were modelled using the formulas of Van Rijn (1984a, 1984b, 1984c), whereas the other two experiments were modelled with the formula of Engelund and Hansen (1967), splitting the total load in two parts at fixed percentages (bed load and suspended sediment load). The suspended sediment transport load was of the same order of magnitude as the bed load, and the modifications to the model are not crucial. The numerical simulations closely follow the measurements except in the run 1 (Figure B.8). For that case the damping is overestimated while the wave length is underestimated.

Table B.2: Flume experiment settings (Talmon, 1992).

| | run 1 | run 2 | run 3 | run 4 |
|---|---|---|---|---|
| $Q$ [$\mathrm{m^3\,s^{-1}}$] | $5.7 \times 10^{-3}$ | $7.7 \times 10^{-3}$ | $5.0 \times 10^{-3}$ | $9.8 \times 10^{-3}$ |
| $i$ [−] | $3.4 \times 10^{-3}$ | $1.7 \times 10^{-3}$ | $2.1 \times 10^{-3}$ | $2.8 \times 10^{-3}$ |
| $h$ [m] | 0.048 | 0.072 | 0.051 | 0.07 |
| $U$ [$\mathrm{m\,s^{-1}}$] | 0.24 | 0.21 | 0.20 | 0.28 |
| $C$ [$\mathrm{m^{0.5}\,s^{-1}}$] | 18.6 | 19.4 | 19.2 | 20.0 |
| $w_s$ [$\mathrm{m\,s^{-1}}$] | $7.6 \times 10^{-3}$ | $7.6 \times 10^{-3}$ | $7.7 \times 10^{-3}$ | $1.7 \times 10^{-2}$ |
| $d_{50}$ [µm] | 88 | 88 | 90 | 160 |
| $\theta_{cr}$ [−] | 0.11 | 0.11 | 0.11 | 0.06 |
| $u_*$ [$\mathrm{m\,s^{-1}}$] | 0.040 | 0.035 | 0.032 | 0.044 |
| $Fr$ [−] | 0.35 | 0.25 | 0.28 | 0.34 |
| $X$ [−] | 0.60 | 0.55 | 0.75 | 0.50 |
| $S_{tot}$ [$\mathrm{m^2\,s^{-1}}$] | $2.5 \times 10^{-6}$ | $9.4 \times 10^{-7}$ | $4.0 \times 10^{-7}$ | $2.9 \times 10^{-6}$ |

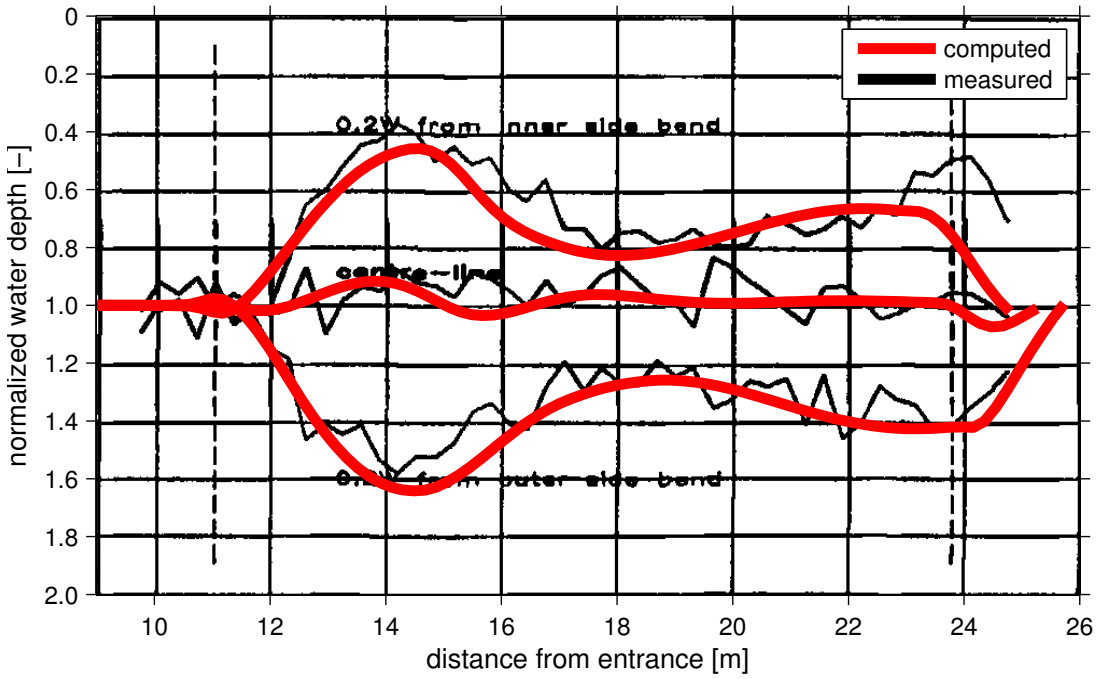


Figure B.8: Run 1 (Talmon, 1992).

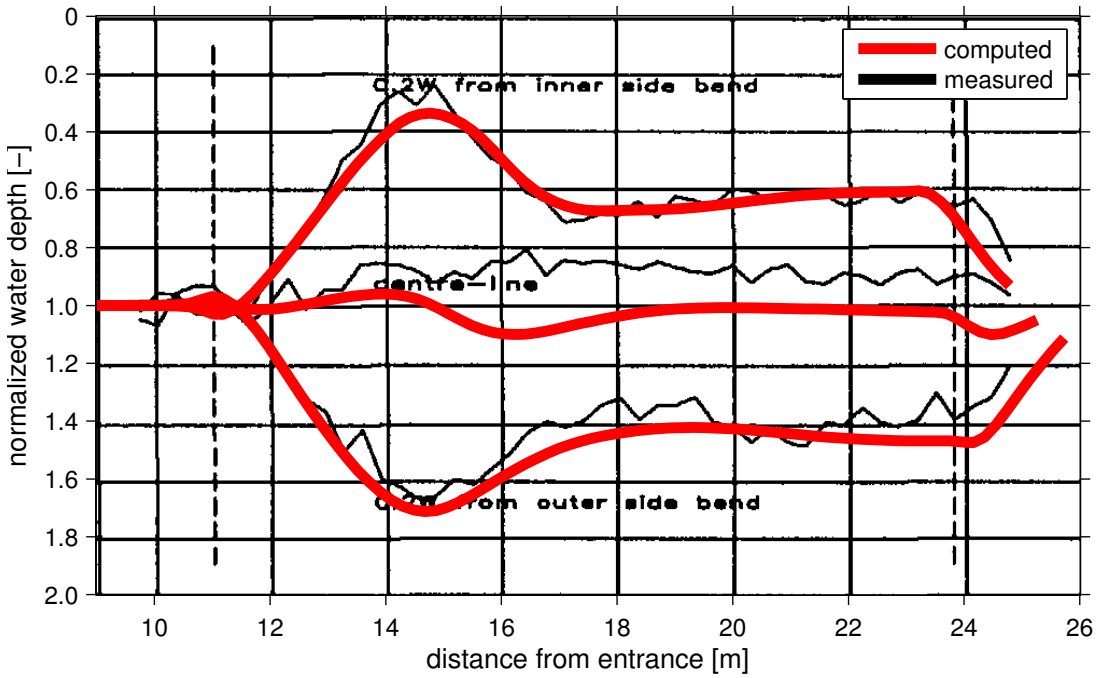


Figure B.9: Run 2 (Talmon, 1992).

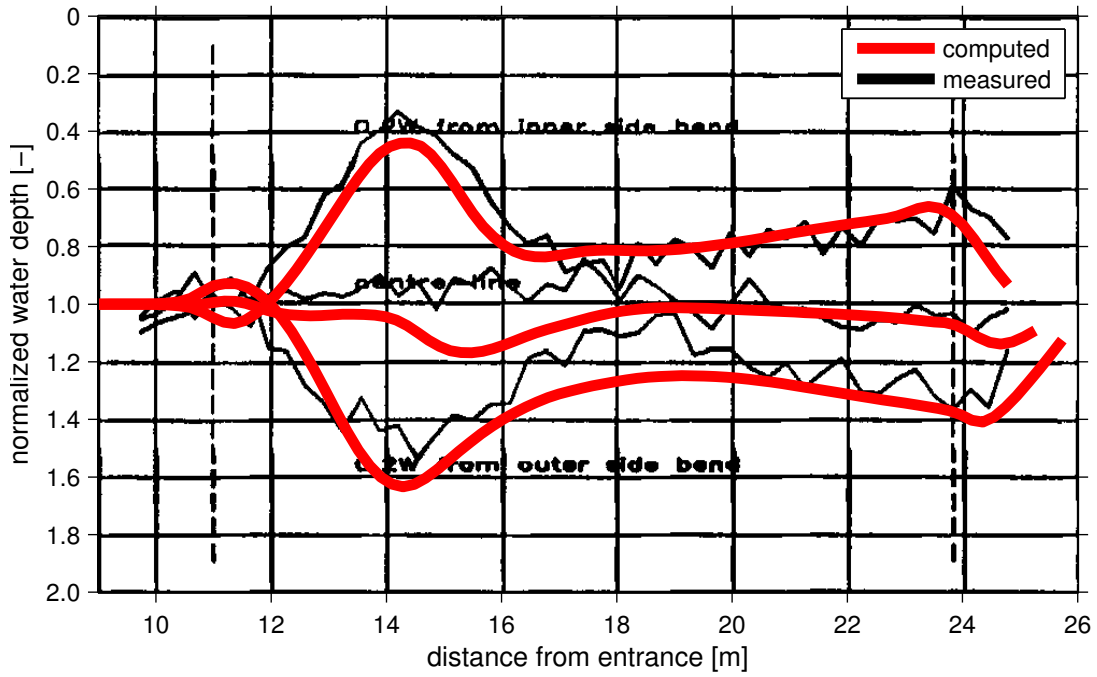


Figure B.10: Run 3 (Talmon, 1992).

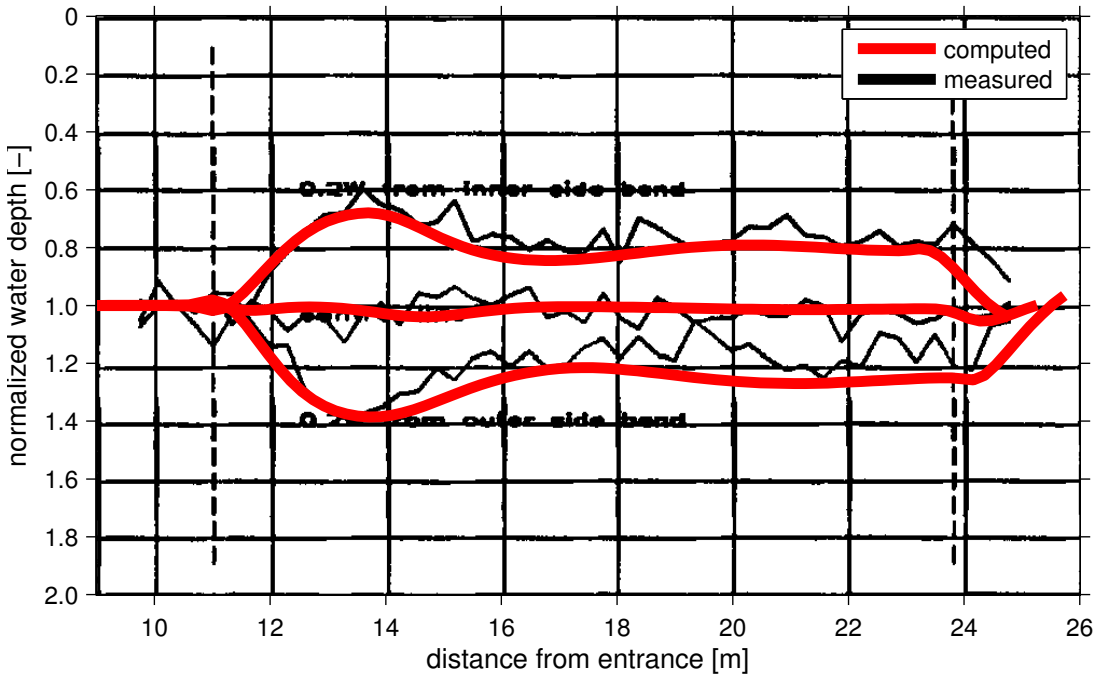


Figure B.11: Run 4 (Talmon, 1992).

### B.1.3 Rio Atrato case study

The settings of the Rio Atrato model are shown in Table B.3. The 3D model consists of 20 non-equidistant layers with increasing height from the bed to the surface. For the modified version of Delft3D, the distribution function for the spiral flow intensity was also included as the banks of the river are modelled as vertical walls.

Table B.3: Data for the Rio Atrato model.

| | Rio Atrato |
|---|---|
| $Q$ | $1517\,\mathrm{m^3\,s^{-1}}$ |
| $h$ | $\approx 8\,\mathrm{m}$ |
| $C$ | $\approx 55\,\mathrm{m^{0.5}\,s^{-1}}$ |
| $d_{50}$ | $350\,\mu\mathrm{m}$ |
| $W$ | $150 - 600\,\mathrm{m}$ |
| $R$ | $200 - 2000\,\mathrm{m}$ |